

Dispersion of motile bacteria in a porous medium

Marco Dentz^{1†}, Adama Creppy², Carine Douarche², Eric Clément^{3,4}
and Harold Auradou²

¹Spanish National Research Council (IDAEA-CSIC), Barcelona, Spain

²Université Paris-Saclay, CNRS, FAST, 91405, Orsay, France

³Laboratoire PMMH-ESPCI Paris, PSL Research University, Sorbonne University, University Paris-Diderot, 7, Quai Saint-Bernard, Paris, France.

⁴Institut Universitaire de France (IUF).

(Received xx; revised xx; accepted xx)

Understanding flow and transport of bacteria in porous media is crucial to technologies such as bioremediation, biomineralization or enhanced oil recovery. While physicochemical bacteria filtration is well-documented, recent studies showed that bacterial motility plays a key role in the transport process. Flow and transport experiments performed in microfluidic chips containing randomly placed obstacles confirmed that the distributions of non-motile bacteria stays compact, whereas for the motile strains, the distributions are characterized by both significant retention as well as fast downstream motion. For motile bacteria, the detailed microscopic study of individual bacteria trajectories reveals two salient features: (i) the emergence of an active retention process triggered by motility, (ii) enhancement of dispersion due to the exchange between fast flow channels and low flow regions in the vicinity of the solid grains. We propose a physical model based on a continuous time random walk approach. This approach accounts for bacteria dispersion via variable pore-scale flow velocities through a Markov model for equidistant particle speeds. Motility of bacteria is modeled by a two-rate trapping process that accounts for the motion towards and active trapping at the obstacles. This approach captures the forward tails observed for the distribution of bacteria displacements, and quantifies an enhanced hydrodynamic dispersion effect that originates in the combined effect of pore-scale flow variability and bacterial motility. The model reproduces the experimental observations, and predicts bacteria dispersion and transport at the macroscale.

1. Introduction

Bacteria are the cause of many diseases and some of them, such as cholera, are spread by contaminated water. In the 19th century, this problem led to the development of drinking water systems separated from wastewater and motivated Darcy to formulate the basic equations describing the flow of a fluid in a porous medium (Darcy 1856). Since then, bacteria transport and filtration through porous media has remained a field of intense research. However, still many practical challenges are concerned with difficulties for macroscopic standard models to provide a reliable and quantitative picture of the dispersion of bacteria transported by flow in porous media. For instance, Hornberger *et al.* (1992) published a study comparing the bacterial effluent curves with those of a

† Email address for correspondence: marco.dentz@csic.es

classical filtration model including fluid convection and absorption-desorption kinetics. The model allows for a good adjustment of the long time tail of the bacteria concentration curves whereas the model gives disappointing predictions for the breakthrough curves at short times. Subsequent studies have sought to identify the influence of flow or physico-chemical conditions on the model parameters. Although little consideration was given to bacterial motility, it came out that this parameter could be crucial to better understand dispersion and retention processes (McCaulou *et al.* 1994; Hendry *et al.* 1999; Camesano & Logan 1998; Jiang *et al.* 2005; Walker *et al.* 2005; Liu *et al.* 2011; Stumpp *et al.* 2011; Zhang *et al.* 2021). Recent studies support the idea that the swimming capacity of the bacteria allows them to explore more of the porosity (Becker *et al.* 2003; Liu *et al.* 2011). For instance, by performing flow experiments with motile and non-motile bacteria in a fracture, Becker *et al.* (2003) recovered at the outlet about 3% of the non-motile bacteria and only 0.6% of similar but motile bacteria. The mass loss of motile bacteria was explained by the fact that motility eases the diffusion into stagnant fluid resulting in a greater residence time in the porosity and close to grain surfaces. As a consequence motile bacteria are more likely to be filtered. This conclusion seems however inconsistent and in contradiction with earlier observations Hornberger *et al.* (1992) and Camesano & Logan (1998) reporting less adhesion to soil grains at low fluid velocity.

Microfluidic technology offers a unique experimental method to directly visualize the behavior of bacteria inside pores. Even when using simple geometries such as channels with rectangular cross sections researchers observed non trivial behavior of bacteria in a flow like upstream motions (Kaya & Koser 2012), back-flow low along corners (Figueroa-Morales *et al.* 2015) eventually leading to large scale "super-contamination" (Figueroa-Morales *et al.* 2020a), transverse motions due to chirality-induced rheotaxis (Marcos *et al.* 2012; Jing *et al.* 2020) and oscillations along the surfaces (Mathijssen *et al.* 2019). Those observations revealed that the dependence of the bacteria orientations on fluid shear adds new elements that further complicate the transport description. Some studies also point out that this dependence might affect the macroscopic transport of motile bacteria suspensions. This was revealed by the experimental study of Rusconi *et al.* (2014). In this work, the bacterial concentration profile across the width of a microfluidic channels was recorded as function of flow velocity. When flow was increased and concomitantly the shear rate, they observed a depletion of the central part of the profile that they attributed to a transverse flux of bacteria from low shear to high shear regions located near the surfaces (Rusconi *et al.* 2014). Motility was also observed to lead to bacteria accumulation at the rear of a constriction (Altshuler *et al.* 2013) or downstream circular obstacles (Miño *et al.* 2018; Secchi *et al.* 2020; Lee *et al.* 2021). Addition of pillars to microfluidic rectangular channels offers the possibility to design model bi-dimensional heterogeneous porous system suited to explore the influence of flow heterogeneities and pore structures on the transport and retention of bacteria (Creppy *et al.* 2019; Dehkharghani *et al.* 2019; Scheidweiler *et al.* 2020; Secchi *et al.* 2020; de Anna *et al.* 2020). This approach allows for tracking of individual bacteria trajectories and the measurement of statistical quantities leading to significant progresses towards the understanding and modeling of bacteria transport and dispersion at a macroscopic scale. They all point out that motility has two major impacts, it increases the residence time close to the grains and in regions of low velocity and favors the adhesion (Scheidweiler *et al.* 2020). The increase of probability to be close to the grains was recently observed in periodic porous media (Dehkharghani *et al.* 2019). The effect on the macroscopic longitudinal dispersion was then investigated numerically using Langevin simulations. Their study revealed a strong enhancement of the dispersion coefficient particularly when the flow is aligned along the crystallographic axis of the porous medium. In this case, the dispersion coefficient is found to increase

like the flow velocity to the power 4 instead of a power 2 as classically obtained for Taylor dispersion. Those examples also show that an accurate macroscopic transport model based on the pore scale observations suited to predict the fate of motile bacteria transported in a porous flow is still missing.

Current approaches to quantify the impact of motility on bacteria dispersion use the generalized Taylor dispersion approach developed by (Brenner & Edwards 1993), which is based on volume averaging of the pore-scale Fokker-Planck equation that describes the distribution of bacteria position and orientation (Alonso-Matilla *et al.* 2019). This approach lumps the combined effect of pore-scale flow variability and motility into an asymptotic hydrodynamic dispersion coefficient. Therefore, it has the same limitations as macrodispersion theory in that it is not able to account for non-Fickian transport features such as forward tails in the distribution of bacteria displacements and non-linear evolution of the displacement variance. The data-driven approach of Liang *et al.* (2018) mimics the run and tumble motion of the bacteria by a mesoscopic stochastic model that represents the motile velocity as a Markov process characterized by an empirical transition matrix, but does not provide an upscaled model equation for bacteria dispersion.

In this paper, our aim is to develop a physics-based mesoscale model for bacteria motion, and derive the upscaled transport equations, by explicitly representing pore-scale flow variability and motility, and their combined impact on bacteria dispersion. In order to understand and quantify the role of motility, we used the experimental data obtained by Creppy *et al.* (2019). Because these experiments were performed at various flow rates and with motile and non-motile bacteria, this data set offers the possibility to investigate the effect of the flow velocity on bacterial motion. We use a continuous time random walk (CTRW) approach (Morales *et al.* 2017; Dentz *et al.* 2018) to model the advective displacements of bacteria along streamlines at variable flow velocities, while the impact of motility is represented as a two-rate trapping process. A similar travel time based approach was used by de Josselin de Jong (1958) and Saffman (1959) to quantify hydrodynamic dispersion coefficients in porous media.

The paper is organized as follows. Section 2 reports on the experimental data for the displacement and velocity statistics of motile and non-motile bacteria. Section 3.1 analyzes transport of non-motile bacteria, which can be considered as passive particles. Thus, we use a CTRW approach, which is suited to quantify the impact of hydrodynamic variability on dispersion. This approach forms the basis for the derivation of a CTRW-based model for the transport of motile bacteria in Section 3.2, which accounts for both hydrodynamic transport and motility. A central element here is to consider and quantify the motility based motion of bacteria toward the solid as an effective trapping mechanism.

2. Experimental data

We use the extensive data set of Creppy *et al.* (2019) for the displacements of non-motile and motile bacteria in a model porous medium consisting of vertical cylindrical pillars placed randomly in a Hele-Shaw cell of height $h = 100\mu\text{m}$, also termed the grains in the following. The pillar diameters were chosen randomly from a discrete distribution (20, 30, 40 and 50 μm) with mean $\ell_0 = 35\mu\text{m}$, which is about 1/3 of the cell height. The grains filled the space with a volume fraction of 33%. This idealized model porous medium shares some characteristics with natural media in channel height and grain size (Bear 1972). A fluorescent *Escherichia coli* RP437 strain is used to facilitate optical tracking. Details on the microfluidic experiments are given in Creppy *et al.* (2019). The raw trajectory data were reanalyzed for this study. We consider data from 7 experiments that are characterized by the mean streamwise velocities of the non-motile bacteria,

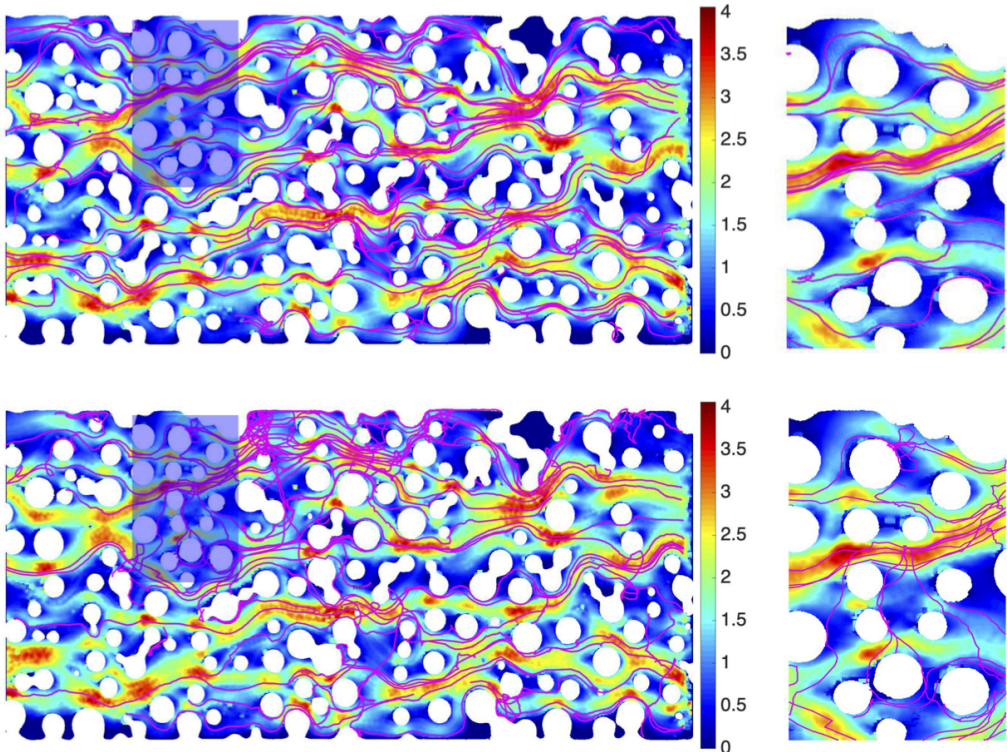


FIGURE 1. Trajectories of motile bacteria at mean velocities (top) $u_m = 98\mu\text{m/s}$ and (bottom) $u_m = 43\mu\text{m/s}$. The shaded area indicates the zoom in the right panel. The color code corresponds to the local fluid velocities with respect to the mean. Velocity data were obtained by tracking passive particles in the flow.

which are $u_m = 18, 43, 66, 98, 113, 139$ and $197\mu\text{m/s}$. In each experiment the motion of both motile and non-motile bacteria are considered. In the following, we refer to the experiments as 18, 43, 66 etc. according to the respective mean velocity. We choose the average grain diameter and the average absolute value of the particle velocity along the flow direction u_m to define the characteristic advection time $\tau_v = \ell_0/u_m$.

2.1. Displacement moments and propagators

Particle trajectories $\mathbf{x}(t) = [x(t), y(t)]$ of different lengths and duration are recorded, along which velocities are sampled, and from which the displacement moments and propagators are determined. Figure 1 illustrates trajectories of non-motile and motile bacteria from the microfluidic experiments. We focus on displacements along the mean flow direction, which is aligned with the x -direction of the coordinate system. Particle displacements are calculated by

$$\Delta x(t_n) = x(t_0 + t_n) - x(t_0), \quad (2.1)$$

where $x(t_0)$ is the starting position of the trajectory at time t_0 and $t_n = n\Delta t$ are subsequent sampling times. The time increment Δt is given by the inverse framerate of the camera. The displacement moments are determined by averaging over all particle

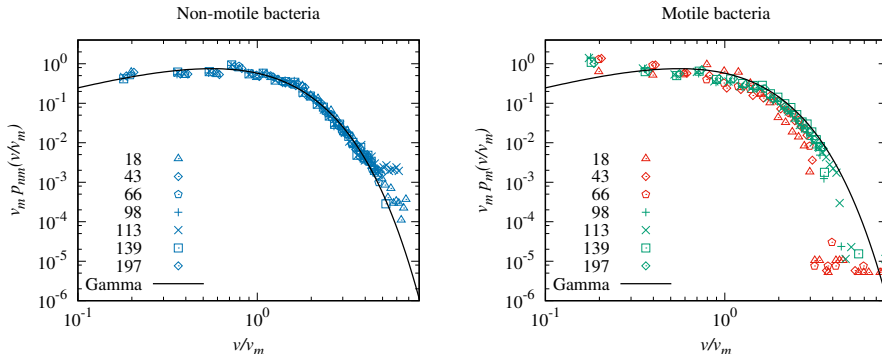


FIGURE 2. Speed distributions for (left) non-motile and (right) motile bacteria for different flow rates rescaled by the mean v_m of the respective non-motile speed distributions. The solid black lines in both figures denotes the analytical approximation by the Gamma distribution (2.6) of the speed distribution for the non-motile bacteria for $\alpha = 2.25$. The legend indicates the experiments, which are identified by the mean streamwise velocity of non-motile bacteria in $\mu\text{m/s}$.

trajectories

$$m_j(t_n) = \frac{1}{N_t} \sum_{k=1}^{N_t} \Delta x_k(t_n)^j, \quad (2.2)$$

where N_t denotes the number of tracks, and subscript k denotes the k th trajectory. The displacement variance is defined in terms of the first and second displacement moments by

$$\sigma^2(t_n) = m_2(t_n) - m_1(t_n)^2. \quad (2.3)$$

The propagators or displacement distribution is defined by

$$p(x, t_n) = \frac{1}{N_t} \sum_{k=1}^{N_t} \frac{\mathbb{I}[x < \Delta x_k(t_n) \leq x + \Delta x]}{\Delta x}, \quad (2.4)$$

where $\mathbb{I}(\cdot)$ is the indicator function, which is 1 if the argument is true and 0 else, Δx is the size of the sampling bin. Note that the number of tracks decreases with track length and sampling time t_n , see the discussion in Appendix A.

2.2. Velocity statistics

Particle velocities $\mathbf{u}(t) = [u_x(t), u_y(t)]$ are obtained from the particle displacements between subsequent images,

$$u_x(t) = \frac{x(t + \Delta t) - x(t)}{\Delta t}, \quad u_y(t) = \frac{y(t + \Delta t) - y(t)}{\Delta t}. \quad (2.5)$$

The particle speed is defined by $v(t) = \sqrt{u_x(t)^2 + u_y(t)^2}$. The mean particle velocity in the following is denoted by $\langle \mathbf{u}(t) \rangle = (u_m, 0)$. The mean speed is denoted by $\langle v(t) \rangle = v_m$. Averages are taken over all tracks and sampling times. The speed PDFs are obtained by sampling over all trajectories and sampling times.

Figure 2 shows the probability density functions (PDFs) of particle speeds for the non-motile and motile bacteria, denoted by $p_{nm}(v)$ and $p_m(v)$, respectively, rescaled by the mean speed v_m of the non-motile bacteria. Non-motile bacteria can be considered passive

tracer particles. Thus, the speed distributions of non-motile bacteria serves as a proxy for the Eulerian flow speed distribution, that is, $p_{nm}(v) \equiv p_e(v)$ which is supported by the fact that the rescaled data collapse on the same curve. The non-dimensional speed data is well represented by the Gamma distribution

$$p_e(v) = \left(\frac{v\alpha}{v_m}\right)^{\alpha-1} \frac{\alpha \exp(-v\alpha/v_m)}{v_m \Gamma(\alpha)}, \quad (2.6)$$

for $\alpha = 2.25$. Speed distributions in porous media are often characterized by exponential or stretched exponential decay for $v > v_m$ and power-law behaviors at low flow speeds. Similar speed distributions have been reported in experimental particle tracking data (Holzner et al. 2015; Morales et al. 2017; Alim et al. 2017; Carrel et al. 2018; Souza et al. 2020) and from numerical simulations of pore-scale flow (Siena et al. 2014; Matyka et al. 2016; De Anna et al. 2017; Aramideh et al. 2018; Dentz et al. 2018).

The right panel of Figure 2 shows the speed PDFs for the motile bacteria rescaled by the mean speed of the respective non-motile bacteria, together with the Gamma distribution given in Eq. (2.6), which models the non-motile speed PDFs. The global shapes of the rescaled speed PDFs for the motile bacteria are very similar to the speed PDF for the non-motile bacteria represented by the Gamma distribution. However, they are shifted towards smaller values when compared to the non-motile bacteria, with a small peak at low values, which can be related to bacteria motion along the grains. The speed PDFs with $u_m \geq 98 \mu\text{m/s}$ scale with the mean speed v_m and group together above all at intermediate and small speeds. The speed PDF of the motile bacteria measures the combined speed of the flow field and bacteria motility. The fact that the speed PDFs collapse when rescaled by the respective mean flow speeds indicates that bacteria motion scales with the flow speed. This seems to be different for the speed PDFs for $u_m \leq 66 \mu\text{m/s}$. The PDFs are more scattered and shifted towards smaller values compared to the speed PDFs for the high flow rates.

Particle trajectories are tortuous due to pore and velocity structures, and thus are longer than the corresponding linear distance. The ratio between the average trajectory length of the non-motile bacteria and the linear length in mean flow direction defines the tortuosity χ . It can be quantified by the ratio between the mean flow speed v_m and the mean flow velocity u_m as (Koponen et al. 1996; Ghanbarian et al. 2013; Puyguiraud et al. 2019b)

$$\chi = \frac{v_m}{u_m}, \quad (2.7)$$

We obtain from the velocity data at all flow rates, tortuosity values between $\chi = 1.17$ and 1.23.

3. Theoretical approach

We present here the theoretical approach to model the dispersion of non-motile and motile bacteria. We use the CTRW framework to model the stochastic motion of bacteria due to pore-scale flow variability and motility, based on a spatial Markov model for subsequent particle velocities, and a compound Poisson process for motility. This type of approach was used to upscale and predict hydrodynamic transport in porous and fractured media at the pore and continuum scales (Berkowitz & Scher 1997; Noetinger et al. 2016; Dentz et al. 2018; Hyman et al. 2019). It naturally accounts for the organization of the flow field along characteristics length scales that are imprinted in the host medium. We focus here on the quantification of the streamwise motion and

| | |
|-------------------------------|---|
| ℓ_0 | grain size |
| ℓ_c | characteristic persistence length of particle speeds |
| ℓ'_c | coarse-graining length |
| v_0 | magnitude of the swimming velocity of the bacteria |
| \mathbf{u} | velocity of non-motile bacteria |
| $v = \mathbf{u} $, | speed of non-motile bacteria |
| $v_m = \langle v \rangle$, | average speed |
| $u_m = \langle u_x \rangle$, | average streamwise velocity |
| $\tau_v = \ell_0/u_m$, | advection time |
| $\chi = v_m/u_m$, | tortuosity |
| τ_c | characteristic trapping time |
| γ | trapping rate |
| D_{nm} | dispersion coefficient of the non-motile bacteria |
| D_m | dispersion coefficient of the motile bacteria |
| ρ | fraction of bacteria at the grains |
| β | partition coefficient |
| R | retardation factor associated to the convection at the macroscopic scale of the motile bacteria |

TABLE 1. Notation

large scale dispersion of bacteria, which play a key role for the prediction of the length of bacteria plumes and the distributions of residence times in a porous medium.

3.1. *Non-motile bacteria*

Non-motile bacteria are considered as passive tracer particles that are transported by advection only. Non-motile bacteria move along streamlines of the porescale flow field, and thus explore the porescale velocity spectrum, except for the lowest velocities close to the grains, due to volume exclusion or molecular diffusion. Typical trajectories are shown in Figure 1. In the following, we model the motion of non-motile bacteria using a spatial Markov model for particle speeds (Dentz et al. 2016; Morales et al. 2017; Puyguiraud et al. 2019b).

3.1.1. *Spatial Markov model*

Particle motion is characterized by the spatial persistence of particle velocities over a characteristic length scale, which is imprinted in the spatial structure of the porous medium (Dentz et al. 2016). This provides a natural parameterization of bacteria motion in terms of travel distance. That is, motion is modeled by constant space and variable time increments along streamlines. Thus, the equations of streamwise motion of non-motile bacteria can be written as (Puyguiraud et al. 2019b)

$$x_{n+1} = x_n + \frac{\Delta s}{\chi}, \quad t_{n+1} = t_n + \frac{\Delta s}{v_n}, \quad (3.1)$$

where Δs is the transition length along the tortuous particle path. The advective tortuosity χ accounts for streamline meandering in the pore space between the grains. It quantifies the ratio of the average streamline length to streamwise distance. Note that this meandering is different for each streamline and may be correlated to the particle speed. However, under ergodic flow conditions, the streamline lengths converge toward the average value, and thus, at scales larger than ℓ_0 tortuosity provides a good estimate for the longitudinal displacement.

The point distribution $p_v(v)$ of particle speeds is given in terms of the Eulerian flow

speed distribution $p_e(v)$

$$p_v(v) = \frac{vp_e(v)}{v_m}. \quad (3.2)$$

This speed-weighting relation is due to the fact that in this framework particles make transitions over constant distance, while the distribution of flow speeds $p_e(v)$ is obtained by measuring speeds at constant framerate, this means isochronically (Dentz et al. 2016; Morales et al. 2017; Puyguiraud et al. 2019b). Equations (3.1) constitute a CTRW because bacteria are propagated over constant (discrete) distances while time is a continuous variable. In this framework, the position $x(t)$ of a particle at time t is given by $x(t) = x_{n_t}$, where $n_t = \max(n | t_n \leq t < t_{n+1})$. The displacement moments are defined by $m_i(t) = \langle x(t)^i \rangle$. The displacement variance is given by $\sigma^2(t) = m_2(t) - m_1(t)^2$.

The series $\{v_n\}$ of particle speeds is modeled as a stationary Markov process whose steady state distribution is given by Eq. (3.2). Specifically, we model $\{v_n\}$ through an Ornstein-Uhlenbeck process for the unit normal random variable w_n which is obtained from v_n through the transformation (Puyguiraud et al. 2019a)

$$w_n = \Phi^{-1} [P_v(v_n)], \quad v_n = P_v^{-1}[\Phi(w_n)], \quad (3.3a)$$

where P_v is the cumulative speed distribution and $\Phi^{-1}(u)$ the inverse of the cumulative unit Gaussian distribution. The w_n satisfies the Langevin equation

$$w_{n+1} = w_n - \ell_c^{-1} \Delta s w_n + \sqrt{2\ell_c^{-1} \Delta s} \xi_n, \quad (3.3b)$$

where ξ_n is a unit Gaussian random variable. The length scale ℓ_c denotes the characteristic correlation scale of particle speed. It is typically of the order of the characteristic grain size ℓ_0 (Puyguiraud et al. 2021). However, its exact value needs to be adjusted from the data for the displacement variance. The increment Δs is chosen such that $\Delta s \ll \ell_c$. The phase-space particle density $p(x, v, t)$ in this framework is given by the Boltzmann-type equation (Comolli et al. 2019)

$$\frac{\partial p(x, v, t)}{\partial t} + v\chi^{-1} \frac{\partial p(x, v, t)}{\partial x} = -\frac{v}{\Delta s} p(x, v, t) + \int_0^\infty dv' r(v, \Delta s | v') \frac{v'}{\Delta s} p(x, v', t), \quad (3.4)$$

see also Appendix B.1. The initial distribution is given by $p(x, v, t = 0) = p_0(x, v) = \delta(x)p_0(v)$, where $p_0(v)$ is the distribution of initial particle velocities. The propagator, that is, the distribution of particle displacements, is given by

$$p(x, t) = \int_0^\infty dv p(x, v, t). \quad (3.5)$$

3.1.2. Asymptotic theory

The behavior of the upscaled model at travel distances much larger than the correlation length ℓ_c , can be obtained by coarse-graining particle motion on a length scale $\ell'_c \geq \ell_c$, such that

$$x_{n+1} = x_n + \frac{\ell'_c}{\chi}, \quad t_{n+1} = t_n + \tau_n, \quad (3.6)$$

The transition times $\tau_n = \ell'_c/v_n$ are independent random variables whose distribution $\psi(t)$ is given in terms of $p_v(v)$ as

$$\psi(t) = \ell'_c t^{-2} p_v(\ell'_c/t) = \left(\frac{t}{\tau_0}\right)^{-2-\alpha} \frac{\exp(-t/\tau_0)}{\tau_0 \Gamma(\alpha+1)}, \quad (3.7)$$

where $\tau_0 = \ell'_c/v_0$. $\psi(t)$ is given here by an inverse Gamma distribution because the particle speed is Gamma-distributed, see Eq. (2.6).

For the velocity distribution (2.6) with $\alpha = 2.25$, the CTRW predicts asymptotically a Fickian dispersion. That is, for times $t \gg \tau_v$, transport can be quantified by the advection-dispersion equation (Dentz & Berkowitz 2003)

$$\frac{\partial p(x,t)}{\partial t} + u_m \frac{\partial p(x,t)}{\partial x} - D_{nm} \frac{\partial^2 p(x,t)}{\partial x^2} = 0. \quad (3.8)$$

with the average velocity $u_m = v_m/\chi$ and the dispersion coefficient (Puyguiraud *et al.* 2021)

$$D_{nm} = \frac{u_m \ell'_c}{2\chi} \frac{\langle \tau^2 \rangle - \langle \tau \rangle^2}{\langle \tau \rangle^2}. \quad (3.9)$$

The mean and mean squared transition times are defined by

$$\langle \tau^k \rangle = \int_0^\infty dt t^k \psi(t) = \tau_0^k \frac{\Gamma(\alpha+1-k)}{\Gamma(\alpha+1)}, \quad (3.10)$$

for $k = 1, 2$. $\Gamma(\alpha)$ denotes the Gamma function. We find by comparison of the dispersion coefficients from the full spatial Markov model and the CTRW model (3.6) that $\ell'_c \approx 1.57\ell_c$.

3.2. Motile bacteria

We provide here the theoretical framework to interpret the trajectory data and motion of motile bacteria. The motion of motile bacteria is due to advection in the flow field and their own motility as illustrated in Figure 1. At zero flow rate, bacteria fluctuate in a random walk-like manner characterized by a zero mean displacement with a characteristic 2D projected swimming velocity $v_0 \approx 12\mu\text{m/s}$ Creppy *et al.* (2019). At finite flow rate, bacteria tend to swim along the streamlines, and make excursions perpendicular to them in order to move toward the solid grains. Based on the observations of Creppy *et al.* (2019) for bacteria motility, we couple the CTRW model for hydrodynamic transport with a trapping approach. These authors found that bacteria move towards the grains at a flow dependent rate γ and dwell on the grain surface for random times θ , which are distributed according to the trapping time distribution $\psi_f(t)$.

3.2.1. Spatial Markov model and trapping

Within the CTRW approach outlined in the previous section, the trapping of bacteria is represented by a compound Poisson process for the time t_n of the bacteria after n CTRW steps. Thus, the equations of motion are given by

$$x_{n+1} = x_n + \frac{\Delta s}{\chi}, \quad t_{n+1} = t_n + \frac{\Delta s}{v_n} + \tau(\Delta s/v_n). \quad (3.11)$$

for $n > 1$. The initial displacement is $x_0 = 0$ for all bacteria. The initial time is set to $t_0 = 0$. The particle speeds v_n evolve according to the process (3.3). The compound

trapping time $\tau(r)$ is given by

$$\tau(r) = \sum_{i=1}^{n_r} \theta_i, \quad (3.12)$$

where θ_i is the trapping time associated to an individual trapping event, and n_r is the number of trapping events during time r . The number of trapping events n_r follows a Poisson process characterized by the rate γ , that is, the mean number of trapping events per CTRW step is $\gamma\Delta s/v_n$. The trapping rate is constant and counts the average number of trapping events per mobile time. While the trapping properties could depend for example on the local flow speeds, we use the Poisson process with constant rate as a robust and simple way of describing the average trapping properties, which is fully defined by the average number of trapping events per mobile time. The distribution of compound trapping times $\tau(r)$, denoted by $\psi_c(t|r)$, can be expressed in Laplace space by (Feller 1968; Margolin *et al.* 2003)

$$\psi_c^*(\lambda|r) = \exp(-\gamma r[1 - \psi_f^*(\lambda)] - \lambda r). \quad (3.13)$$

$\psi_c(t|r)$ denotes the probability that the trapping time is t given that a trapping event occurred at time r . For $n = 1$, we distinguish the proportion ρ of bacteria that are initially trapped, and $1 - \rho$ of initially mobile bacteria. For the trapped bacteria, $x_1 = 0$ and $t_1 = \eta_0$, where the initial trapping time η_0 is distributed according to $\psi_0(t)$. For the mobile bacteria, x_1 and t_1 are given by Eq. (3.11) for $n = 0$.

We consider here steady state conditions at time $t = 0$. As experimental trajectories and their starting points are recorded continuously, it is reasonable to assume that steady state between mobile and immobile bacteria is attained. Under steady state conditions, the joint probability of the bacterium to be trapped and the initial trapping time to be in $[t, t + dt]$ is

$$P_0(t) = \int_t^\infty dt' \gamma \exp[-\gamma(t' - t)] \psi_f(t') \quad (3.14)$$

see Appendix C. The trapping times are assumed to be exponentially distributed, that is,

$$\psi_f(t) = \exp(-t/\tau_c)/\tau_c \quad (3.15)$$

with τ_c the characteristic trapping time. This means, we use Poissonian statistics to account for the effective retention of motile bacteria in the vicinity of grain surfaces. This picture is classically based on the idea that the run to tumble process promoting surface detachment is itself a memory-less Poisson process (Berg 2018). However, there has been recent evidence that the run-time distribution for bacterial motion in a free fluid is a long-tail non-Poissonian process (Figueroa-Morales *et al.* 2020b), which is also at the origin of a long-tailed distributions of bacteria sojourn times at flat surfaces (Junot *et al.* 2021). For porous media, there are currently no direct measurements that offer a quantitative microscopic description of the complex exchange processes taking place between the surface regions and the flowing regions. Thus, we adopt Poissonian statistics characterized by the mean retention time τ_c as a model of minimal assumptions. We hope that our conceptual approach, which provides a model of the emerging transport process, will motivate more detailed experimental investigations on this central question.

Using Eq. (3.15) in Eq. (3.14), we obtain

$$P_0(t) = \frac{\beta}{1 + \beta} \frac{\exp(-t/\tau_c)}{\tau_c}, \quad (3.16)$$

where we define the partition coefficient $\beta = \gamma\tau_c$. Thus, the fraction of trapped bacteria is $\rho = \beta/(1 + \beta)$, and the initial trapping time distribution is $\psi_0(t) = \psi_f(t)$. Thus, the steady state partitioning of bacteria is directly related to their motility through the trapping rate γ and mean dwelling time τ_c on the grain surface.

Note that this picture does not account for the tortuous particle path on the grain surfaces, which is represented as a localization event at fixed positions. Grain-scale bacteria motility could eventually be modeled by an additional process. However, here we focus on large scale bacteria dispersion and only account for tortuosity due to the flow path geometry. As above the bacteria position $x(t)$ at time t is given by $x(t) = x_{n_t}$. The expressions for the displacement moments and variance are analogous.

The density $p_s(x, v, t)$ of mobile bacteria in the stream is quantified by the non-local Boltzmann equation

$$\begin{aligned} \frac{\partial p_s(x, v, t)}{\partial t} + \frac{\partial}{\partial t} \int_0^t dt' \gamma \phi(t - t') p_s(x, t') + \frac{v}{\chi} \frac{\partial p_s(x, v, t)}{\partial x} = \\ \rho \delta(x) p_0(v) \psi_f(t) - \frac{v}{\Delta_s} p_s(x, v, t) + \int_0^\infty dv' r(v|v') \frac{v'}{\Delta_s} p_s(x, v', t'), \end{aligned} \quad (3.17)$$

see Appendix B.2. We defined

$$\phi(t) = \int_t^\infty dt' \psi_f(t'), \quad (3.18)$$

the probability that the trapping time is larger than t . Equation (3.17) reads as follows. The evolution of the particle density in the stream is given by (second term on the left side) particle exchange between the stream and grain surface, (third term on the left) advection by the local velocity, (first term on the right side) release of bacteria that were initially on the grains, (second and third terms on the right) velocity transitions along the trajectory.

The total bacteria density is given by

$$p(x, v, t) = p_s(x, v, t) + p_g(x, v, t). \quad (3.19)$$

The density $p_g(x, v, t)$ of bacteria on the grains is given by

$$p_g(x, v, t) = \int_0^t dt' \phi(t - t') \gamma p_s(x, v, t') + \delta(x) \rho \phi(t) p_0(v) \quad (3.20)$$

This first term on the right side reads as follows. The density of bacteria on the grains is given by the probability per time $\gamma p_s(x, t')$ that bacteria are trapped at time t' times the probability $\phi(t - t')$ that the trapping time is longer than $t - t'$. The second term denotes the bacteria that are initially trapped and whose trapping time is larger than t . The speed v associated with a bacterium on the grain should be understood as the bacteria speed before the trapping events.

3.2.2. Asymptotic theory

Similar to the discussion in the previous section for the non-motile bacteria, for distances much larger than ℓ_c , particle motion can be coarse-grained such that

$$x_{n+1} = x_n + \ell'_c, \quad t_{n+1} = t_n + \tau_n + \tau(\tau_n), \quad (3.21)$$

where the advective transition times $\tau_n = \ell'_c/v_n$ are distributed according to Eq. (3.7). $\tau(r)$ describes the compound Poisson process defined above. The propagator $p_s(x, t)$ of bacteria in the stream for this equation of motion is quantified by the non-local advection-dispersion equation

$$\begin{aligned} \frac{\partial p_s(x, t)}{\partial t} + \frac{\partial}{\partial t} \int_0^t dt' \gamma \phi(t - t') p_s(x, t') \\ + u_m \frac{\partial p_s(x, t)}{\partial x} - D_{nm} \frac{\partial^2 p_s(x, t)}{\partial x^2} = \rho \delta(x) \psi_f(t), \end{aligned} \quad (3.22)$$

while the distribution $p_g(x, t)$ of bacteria at the grains is given by

$$p_g(x, t) = \int_0^t dt' \phi(t - t') \gamma p_s(x, t') + \delta(x) \rho \phi(t). \quad (3.23)$$

Asymptotically this means for times $t \gg \tau_c$, the transport of the bacteria concentration $p(x, t)$ can be described by the advection-dispersion equation

$$\frac{\partial p(x, t)}{\partial t} + \frac{u_m}{R} \frac{\partial p_s(x, t)}{\partial x} - D_m \frac{\partial^2 p_s(x, t)}{\partial x^2} = 0, \quad (3.24)$$

see Appendix D. The retardation coefficient R and the asymptotic dispersion coefficient D_m are given by the explicit expressions

$$R = 1 + \gamma \tau_c = \frac{1}{1 - \rho}, \quad (3.25)$$

$$D_m = D_{nm}(1 - \rho) + u_m^2 \tau_c \rho (1 - \rho)^2. \quad (3.26)$$

By definition, R compares the average velocity of motile bacteria with the average flow velocity. In absence of trapping, $\rho = 0$ and $R = 1$, the bacteria are transported in the porous media with an average velocity equal to the average fluid velocity. If trapping is present, retardation increases, indicating a decrease of the average bacteria velocity compared to the fluid velocity. The retardation coefficient is directly related to bacterial motility, which in our modeling framework is expressed by the trapping rate γ and the mean retention time τ_c for which a bacterium dwells at the grain surface.

The asymptotic dispersion coefficient in Eq. (3.26) contains two terms. The first term $D_{nm}(1 - \rho)$ corresponds to the so-called dispersion coefficient at steady state (Yates et al. 1988; Tufenkji 2007). It predicts a reduction of the dispersion coefficient of the motile bacteria compared to the non-motile concomitant with the reduction of the average velocity of the bacteria population. It accounts for the dispersion of the motile proportion $1 - \rho$ only. The second term quantifies a mechanism similar to the Taylor dispersion. It originates from the spread of the bacteria plume due to fast transport in the pores and localization at the grains. The resulting dispersion effect can be rationalized as follows. The typical separation distance between localized and mobile bacteria, that is, the dispersion length is $u_m \tau_c$, while the dispersion time is τ_c . The corresponding dispersion coefficient is dispersion length squared divided by dispersion time, which gives exactly

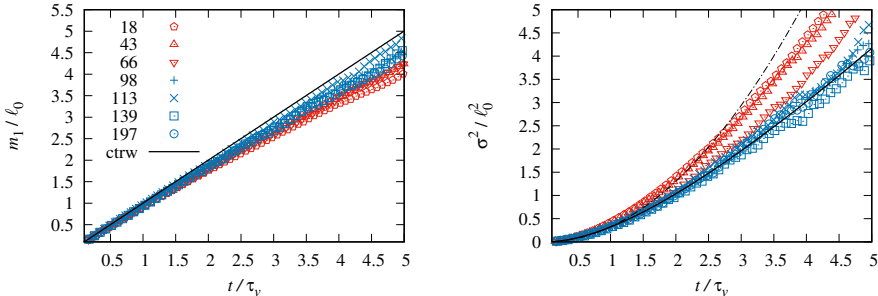


FIGURE 3. (Left panel) Normalized mean displacements and (right panel) normalized displacement variances for non-motile bacteria as a function of normalized time. The solid lines denote the estimate from the CTRW model. The dash-dotted line in the right panel indicates the initial ballistic growth.

the scaling $u_m^2 \tau_c$ of Eq. (3.26). As we will see in the next section, this interaction can lead to a significant increase of bacteria dispersion compared to non-motile bacteria.

Asymptotic bacteria transport is predicted to obey the advection-dispersion equation with constant parameters for two reasons. First, the distribution of particle velocities does not tail towards low values, that is, mean and mean squared transition times are finite. Second, the distribution of retention times is exponential. Thus, for times large compared to the characteristic mass transfer times, the support scale can be considered as well-mixed, and, similar to Taylor dispersion (Taylor 1953), and generalized Taylor dispersion (Brenner & Edwards 1993), transport can be described by an advection-dispersion equation.

4. Results

We discuss the experimental results for the displacement means and variances, as well as the displacement distributions, in the light of the theory presented in the previous section. As discussed in Appendix A, the number of experimentally observed tracks decreases with the travel time, which introduces a bias toward slower bacteria. Thus, in the following, we consider travel times shorter than $5\tau_v$ in order to avoid a too strong bias toward slow bacteria. Even so, as we will see below, there is a slowing down of the mean displacement with increasing travel time, specifically for the motile bacteria.

The proposed theoretical approach for the non-motile bacteria has one parameter that needs to be adjusted, the correlation scale ℓ_c , which typically is of the order of the grain size. It is adjusted here from the data for the displacement variance for the non-motile bacteria. The approach for the motile bacteria has two additional parameters, the trapping rate γ and the mean trapping time τ_c . The partition coefficient $\beta = \gamma\tau_c$ is adjusted from the mean displacement data for the motile bacteria, while the trapping time τ_c is adjusted from the data for the displacement variance of the motile bacteria. Thus, the non-motile CTRW model needs to adjust one parameter, which is of the order of the grain size. The motile CTRW model needs to adjust two parameters, which are related to the partitioning of bacteria between flowing and stagnant regions close to the grains.

4.1. Dispersion of non-motile bacteria

Figures 3 and 4 show displacement means and variances and the propagators for non-motile bacteria at different flow rates and for the same dimensionless times. Time is

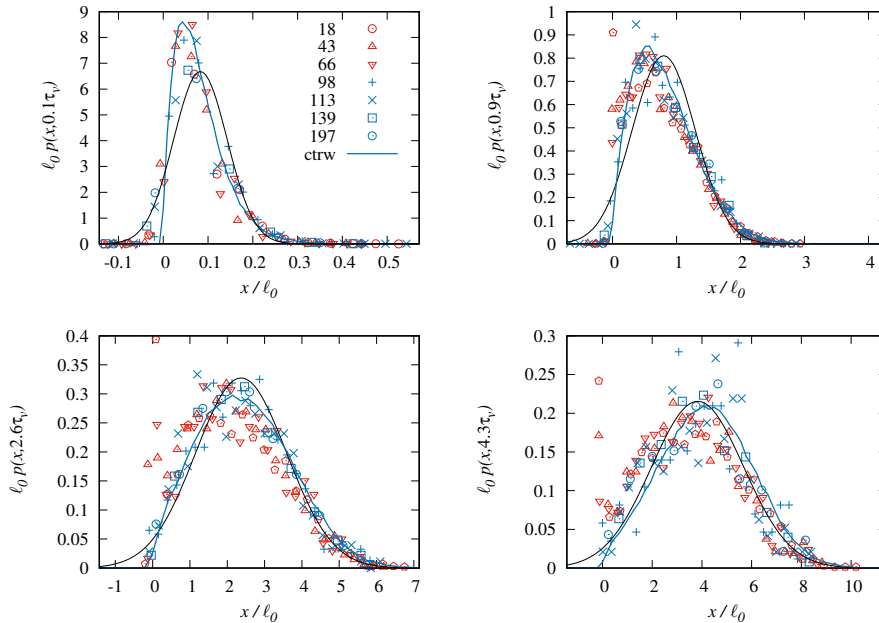


FIGURE 4. Propagators of non-motile bacteria at (left to right) $t = 0.1, 0.9, 2.6, 4.3\tau_v$. The blue solid lines denote the prediction of the CTRW model, the black lines are the fits from the Gaussian transport model that is characterized by the corresponding measured displacement mean and variance shown in Figure 3.

non-dimensionalized by the mean advection time over the size of a grain, which implies that the propagators are reported for the same mean travel distances. The CTRW model uses the velocity distribution (2.6) with $\alpha = 2.25$, the correlation length $\ell_c \approx 2\ell_0$ and the advective tortuosity $\chi = 1.2$.

The mean displacement is linear with a slightly higher slope at short than at large times. It starts deviating from the expected behavior $m_1(t) = u_m t$ at around $t = 2\tau_v$. We relate this behavior to a bias due to the decrease in the number of tracks as discussed in Appendix A. The displacement variance shows a ballistic behavior at $t < \tau_v$, this means it increases as t^2 . Then for $t > \tau_v$ it increases superlinearly, which can be seen as a long cross-over to normal behavior. These behavior are accounted for by the CTRW model. For flow velocities $u_m \leq 66 \mu\text{m/s}$, we observe a larger variance than for the higher flow rates. This, and the slightly smaller mean displacements compared to higher flow rates, can be attributed to the localization of some bacteria at the origin (see Figure 4), which causes a chromatographic dispersion effect, which is discussed in more detail for the motile bacteria.

Figures 4 compares the experimental data for the propagators with the results of the CTRW model. The propagators are asymmetric but compact, meaning that there is no significant forward or backward tails in the distribution. For comparison, we plot a Gaussian shaped propagator characterized by the mean displacement and displacement variance shown in Figure 3. The asymmetry decreases with increasing travel time and the propagators become closer to the corresponding Gaussian. The CTRW model captures the initial asymmetry and the transition to symmetric Gaussian behavior for all flow rates.

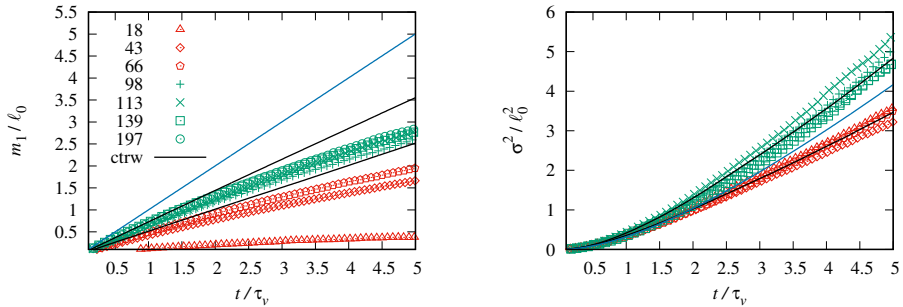


FIGURE 5. (Left panel) Normalized mean displacements and (right panel) normalized displacement variances for motile bacteria, as a function of normalized time. The experimental data are denoted by the symbols, the corresponding CTRW model results by the thick solid lines. The CTRW model uses $\tau_c = 2.5\tau_v$ and $\beta = \gamma\tau_c = 0.4$ for $u_m \geq 98\mu\text{m/s}$ and $\tau_c = 2\tau_v$ and $\beta = 1$ for $u_m = 66\mu\text{m/s}$. The solid blue lines denote the model outcomes for the non-motile bacteria.

4.2. Dispersion of motile bacteria

Figures 5, 6 and 7 show the displacement mean and variance, and the propagators for the motile bacteria at different flow rates. As in the previous section, time is measured in units of τ_v , that is, it measures the mean number of grains the bacteria have passed. The propagators are measured at the same non-dimensional times, that is, at the same mean distance. The motile CTRW model is parameterized by the same correlation length and tortuosity as the non-motile model. The partition coefficient $\beta = \gamma\tau_c$ is adjusted from the early time behavior of the mean displacement, which is predicted to behave as

$$m_1(t) = \frac{u_m t}{R} = \frac{u_m t}{1 + \beta}, \quad (4.1)$$

because we consider the system to be initially in a steady state. The characteristic trapping time is adjusted from the displacement variance by keeping β fixed. We adjust $\tau_c = 2.5\tau_v$ and $\beta = \gamma\tau_c = 0.4$ for $u_m \geq 98\mu\text{m/s}$, and $\tau_c = 2\tau_v$ and $\beta = 1$ for $u_m = 66\mu\text{m/s}$.

As shown in Figure 5, the mean displacement is consistently lower for the motile than for the non-motile bacteria, which is due to migration toward the grain surfaces and localization at the grains. The mean displacement initially evolves linearly until a time of about $2\tau_v$ and from there, the evolution slows down. We relate this to the decrease of the number of experimentally observed tracks, which induces a bias toward slow tracks as discussed in Appendix A. In contrast to the mean displacement, the displacement variance can be larger than its non-motile counterpart for $u_m \geq 98\mu\text{m/s}$ and lower for $u_m \leq 66\mu\text{m/s}$. The data seem to fall into two groups for high and low flow rates, except for $u_m = 18\mu\text{m/s}$. In this case, the flow velocity is of the order of the swimming velocity $v_0 \approx 12\mu\text{m/s}$. The data indicates that the density of trapped particles is higher at high than at low flow rates. The possible mechanisms for these behaviors are discussed in Section 5.

These behaviors are also reflected in the propagators shown in Figure 6 for high flow rates with $u_m \geq 98\mu\text{m/s}$ and in Figure 7 for $u_m \leq 66\mu\text{m/s}$. The green symbols in Figure 6 denote the experimental data rescaled by the mean grain size ℓ_0 , the solid green lines, the corresponding solution from the CTRW model for the parameters $\tau_c = 2.5\tau_v$ and $\beta = \gamma\tau_c = 0.4$. Analogously, the red symbols in Figure 7 denote the experimental data rescaled by the mean grain size ℓ_0 . The solid red lines show the corresponding solution from the CTRW model for the parameters $\tau_c = 2\tau_v$ and $\beta = 1$. For comparison, we also

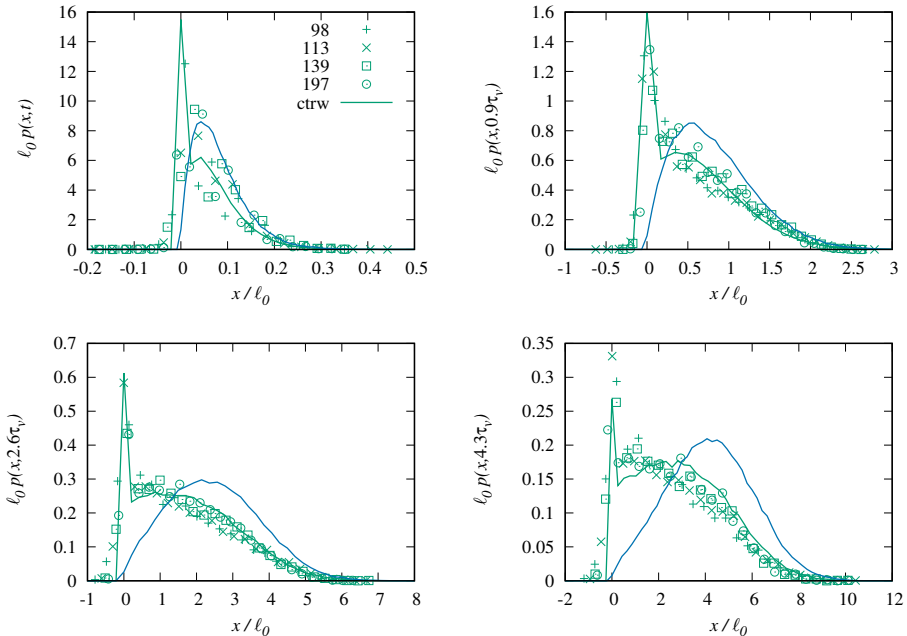


FIGURE 6. Distributions of motile bacteria for high flow rates at (left to right) $t = 0.1, 0.9, 2.6, 4.3\tau_v$. The blue solid lines denote the corresponding predictions of the CTRW model for the non-motile bacteria.

plot the corresponding CTRW solution for the non-motile bacteria, marked by the blue solid lines. The motile propagators are delayed compared to the non-motile bacteria. They are characterized by a localized peak around zero and a pronounced forward tail, which can be attributed (i) to slow motion towards and around grains and (ii) to fast motion in the main pore channels. Figure 6 shows that the propagators at high flow rates ($u_m \geq 98\mu\text{m/s}$) overlap, which indicates that bacteria motion scales with the mean flow. Similarly, for the low flow rates ($u_m \leq 66\mu\text{m/s}$) shown in Figure 7, we observe overlap in the forward tails, which are advection-dominated due to transport in the pore-channels. However, the upstream tails that develop starting from the localized peak do not group together. They can be attributed to bacteria motility, which is independent of the flow rate. This is most pronounced for $u_m = 18\mu\text{m/s}$, which is characterized by strong localization and an almost symmetric propagator. The features of peak localization and forward tailing show that steady state in the macroscopic transport behavior has not been attained at the largest observation time. At asymptotic times, that is, for $t \gg \tau_c$, the theoretical model given by Eq. (3.24) predicts Fickian transport characterized by symmetric propagators.

The data for the displacement moments and propagators seems to indicate that the data are grouped in two families, which we have highlighted by using two different colors. These observations are in agreement with the behaviors of the speed PDFs shown in Figure 2. We therefore fit each family separately. From the early time evolution of the mean displacements, we adjust the partition coefficient $\beta = 0.4$ for $u_m \geq 98\mu\text{m/s}$, $\beta = 1$ for $u_m \leq 66\mu\text{m/s}$. For $u_m \geq 98\mu\text{m/s}$, we adjust from the displacement data $\tau_c = 2.9\tau_v$ and for $u_m = 66\mu\text{m/s}$, we adjust $\tau_c = 2.3\tau_v$.

With these parameter sets, the CTRW model is able to describe the propagators and displacement moments as shown in Figures 5 and 6. For the lowest flow velocity, bacteria

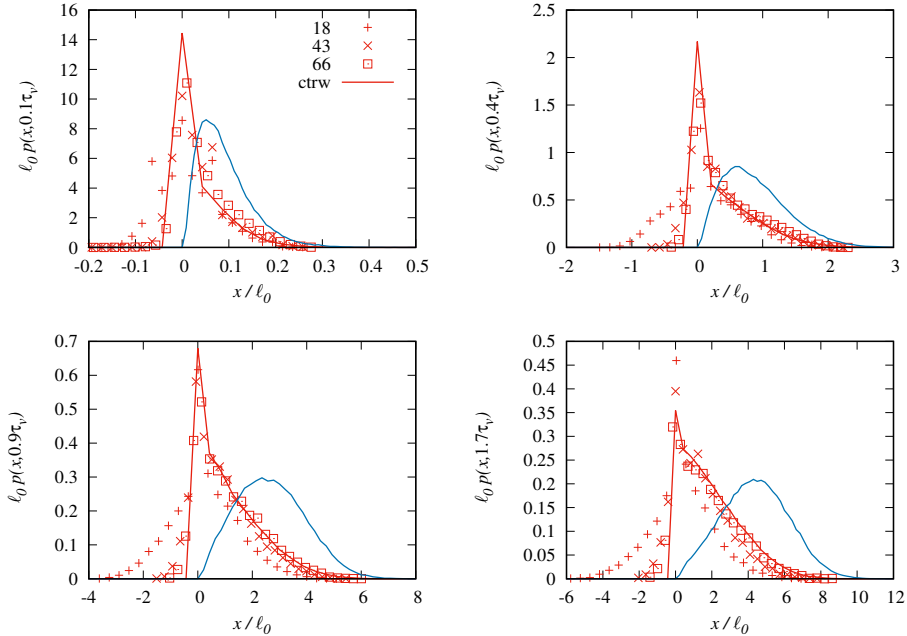


FIGURE 7. Propagators of motile bacteria for low flow rates at (left to right) $t = 0.1, 0.9, 2.6, 4.3\tau_v$. The blue solid lines denote the prediction of the CTRW model for the non-motile bacteria.

are able to swim upstream over relatively long distances. The subsequent backward tail that develops because of the upstream motion is clearly visible in Figure 6 (bottom row), and also, to a smaller extent at the higher flow rates (top row). This effect is not accounted for in the model that assumes that the trapping is localized and that trapped bacteria do not move once trapped.

Since $\tau_v \propto 1/u_m$, our results indicate that the trapping rate increases linearly with the average flow velocity u_m while the characteristic trapping time decreases linearly with u_m . We used different values for $\beta = \gamma\tau_v$ and τ_c to adjust the two sets. Recall that the fraction of trapped bacteria ρ is $\beta/(1 + \beta)$. Each set thus corresponds to a different value of the fraction of trapped bacteria. The fraction of trapped bacteria is high at low velocities ($\rho \geq 0.5$) and decreases towards an asymptotic value of about $\rho = 0.3$ as the flow velocity is increased. The fraction of trapped bacteria is also related to the retardation coefficient R through Eq. (3.25), which is estimated from the experimental data for the mean bacteria displacement according to relation (4.1). The dependence of R and thus ρ on the flow rate is further discussed in the next section.

4.3. Asymptotic dispersion and retardation

The CTRW model allows to extrapolate the transport behaviors to times that cannot be reached in the experiment. The top panels of Figure 8 show the displacement mean and variance up to times of $1000\tau_v$. We see that both observables evolve linearly at asymptotic times. The mean displacement indicates a lower average velocity for the motile than for the non-motile bacteria, which is due to trapping. The displacement variance on the other hand is larger for the motile than for the non-motile at high flow rates, which indicates stronger motile dispersion. This effect can be quantified by Eqs. (3.25) and (3.26) for the retardation coefficient and asymptotic dispersion coefficient.

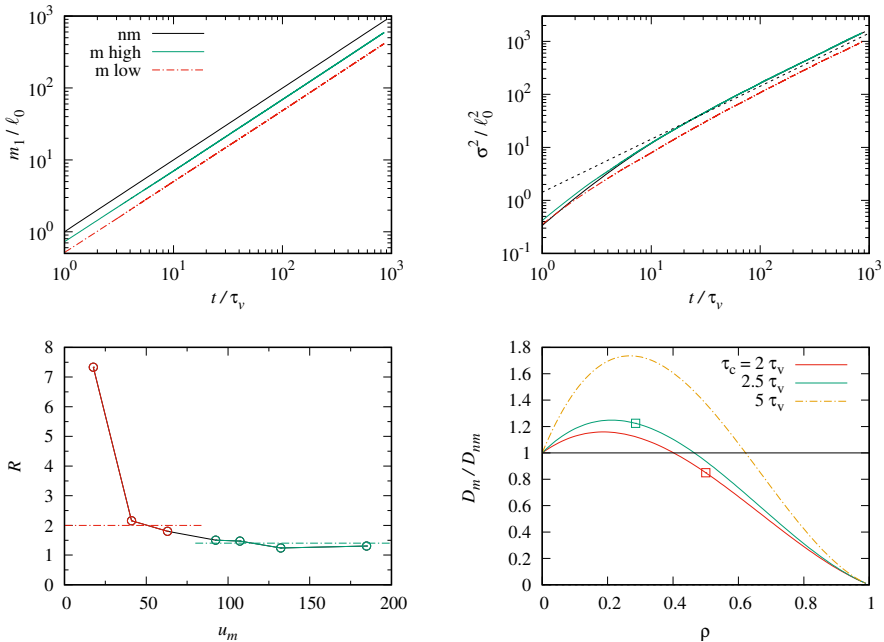


FIGURE 8. Top panel: Model predictions for the displacement (left) means and (right) variances of motile and non-motile bacteria. Bottom panel left: retardation coefficient from experimental data. The dash-dotted line indicates the values used in the CTRW model at (green) high and (red) low flow rates. Bottom panel right: Dispersion coefficient for the motile bacteria as a function of the fraction ρ of trapped bacteria for $\tau_c = 2\tau_v, 2.5\tau_v, 5\tau_v$. The squares denote the dispersion coefficient at the ρ -values for (green square) $u_m \geq 98\mu\text{m/s}$ and (red square) $u_m = 66\mu\text{m/s}$.

The retardation coefficient $R = 1/(1 - \rho) = 1 + \beta$ can be estimated directly from the experimental data for the mean displacement according to Eq. (4.1). The left panel at the bottom of Figure 8 shows that the retardation coefficient decreases with increasing flow rate, which is consistent with the values adjusted for β in the previous section. Thus the data shows also that the fraction ρ of trapped particles decreases with increasing flow rate.

The behavior of D_m as a function of the proportion ρ of trapped bacteria is shown in the bottom panel of Figure 8. The solid line shows the theoretical behavior of D_m for $\tau_c = 2.5\tau_v$ and $\tau_c = 2\tau_v$, which corresponds to the value used in the CTRW model. The green and red symbols denote the values obtained from the CTRW models at high and low flow rates. We see that at low fractions of immobile bacteria, the Taylor term in Eq. (3.26) dominates and motile bacteria disperse more than non-motile. At high proportions of trapped bacteria, localization dominates over the Taylor mechanism, and motile dispersion is lower than non-motile. Figure (8) illustrates the competition between the trapping time τ_c and the proportion ρ of trapped bacteria. For increasing τ_c , motile dispersion can be significantly larger than non-motile dispersion.

5. Discussion

We study the interaction between bacteria motility and flow variability, and its impact on the dispersion of bacteria. To do so we use data obtained in a microfluidic chip containing randomly placed obstacles, in which thousands of non-motile and motile

bacteria were tracked at different flow rates. This geometry reproduces the structure of a porous medium on the scale of a few pores, and is thus ideal to study transport phenomena at the pore scale. Because bacteria do not adhere to the surface of the flow cell, this setup allows to study the first step of filtration which consists of the transport of bacteria from the flowing fluid to regions of low flow in the vicinity of solid grains.

Bacteria motion is quantified by a CTRW approach that is based on a Markov model for equidistant particle speeds. The experimental data for the displacement of non-motile bacteria is used to constrain the velocity correlation length, which is of the order of the grain size. Bacteria motility is modeled in this framework by a trapping process, which accounts for the rheotactic motion toward and along the grain surfaces by a trapping rate γ and characteristic dwelling time τ_c . The ratio between trapped and mobile bacteria at steady state is measured by the partition coefficient $\beta = \gamma\tau_c$.

Adjustment of the model to the experimental data reveals two main features. Firstly, we observe that $\gamma \propto u_m$ and $\tau_c \propto 1/u_m$. The increase of the trapping rate with the flow rate can be explained by the constant reorientation of the bacteria by the flow. The frequency by which bacteria point toward the grains increases with the flow rate, which may explain the increase of the trapping rate. Similarly, for increasing flow rate, shear increases on the grains and thus the area for motion around the grains decreases and the bacteria are more easily blown off by the flow. This can explain why the residence time decreases with flow rate. A model that supports this idea is proposed in Appendix E.

Secondly, we observe that the ratio β between trapped and mobile bacteria is different at high and low flow rates. This observation indicates a transition between a regime at low flow rates, where motility favors trapping with a high density of trapped bacteria (about 50% of trapped bacteria), to a regime at high flow rates, where the flow hinders trapping (about 30% of trapped bacteria). Two phenomena may contribute to this change. The first comes from the volume of fluid in which the bacteria can be considered as trapped. This fraction can be separated in two: a part where the velocity is very small (this part corresponds to the dark blue regions that can be seen in Figure 1 and is always present for all the flow rates used) and a second contribution which comes from the regions of flowing fluid where the average flow velocity is less than the swimming velocity. In those volumes, which are located close to the grain surface the bacteria trajectories are little influenced by the flow and they swim much like in a quiescent fluid. Bacteria can be considered trapped when they swim along the grain surface. This contribution however decreases with the flow rate reducing in turn the density of trapped bacteria as observed. The second contribution comes from the diffusion due to the constant reorientation of the bacteria. In a fluid at rest, the trajectories of the bacteria can be decomposed as a succession of runs followed by tumbles that reorient the bacteria. At large scale, the reorientation is diffusive and can be characterized by the translational diffusion coefficient D_b . For E.coli we have here $D_b \approx 243\mu\text{m}^2/\text{s}$ (Creppy et al. 2019). In a shear flow, bacteria constantly tumble and are reoriented at a frequency set by the shear rate $\dot{\gamma}$ (Jeffery 1922). When the Péclet number defined as $Pe = u_m\ell_0/2D_b$ is of the order of 1. For a grain size of $\ell_0 = 30\mu\text{m}$, we have $Pe \simeq u_m/(16\mu\text{m}/\text{s})$. Random orientation will thus dominate shear alignment for the lowest flow rate with little or no influence at high flow velocity.

6. Conclusions

In conclusion, to understand the dispersion of bacteria in porous media, our study focuses on the central importance of hydrodynamic flow fluctuations and the active exploration process into high shear regions around the solid grains. The rheotactic coupling between flow and bacteria motility manifests itself at small scales through

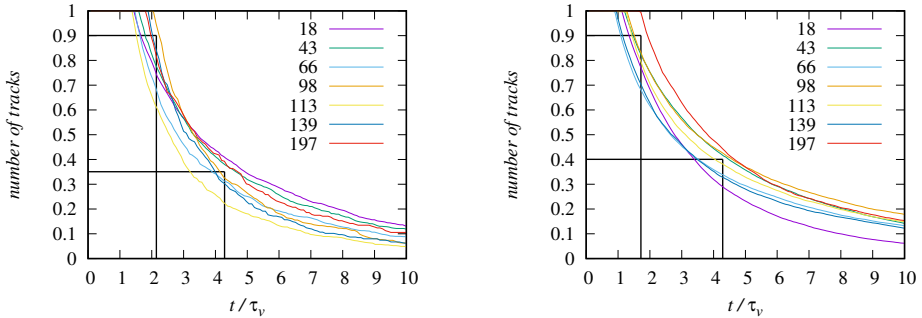
non-Fickian behavior, and at large scales through a motility-dependent hydrodynamic dispersion effect. Noticeably, the interplay between fast transport in the flow and motile motion toward grain surfaces is the first necessary step before possible adhesion (Yates et al. 1988). To date, it had been assumed that the transfer between regions of high fluid flow and low flow regions in the vicinity of the grain surfaces was diffusive, like for passive solutes, and had been modeled as a kinetic single-rate mass transfer process (Yates et al. 1988; Bai et al. 2016). Our study suggests that both motility and flow play a central role in the trapping and release processes, which are characterized by two different rates. Both trapping and release rates are proportional to the average flow velocity, while the ratio between mobile and trapped particle increases with increasing flow velocity. The trapping and release mechanisms explain apparently contradictory observations of the concomitant enhancement of retention and dispersion. They are quantified in a theoretical approach that captures the salient features of the experimental displacement data, and allows for predicting the dispersion of motile bacteria at large scales. These findings shed light on the strategies microorganisms may use to maximize their survival and proliferation abilities under natural conditions, and can give new insights into bacteria filtration and biofilm growth, for which the contact with grain surfaces is determinant.

Acknowledgments

M.D. acknowledges the support of the Spanish Research Agency (10.13039/501100011033) and the Spanish Ministry of Science and Innovation through the project HydroPore (PID2019-106887GB-C31). H.A and C.D. acknowledge the support of the “Laboratoire d’Excellence Physics Atom Light Mater” (LabEx PALM) as part of the “Investissements d’Avenir” program (reference: ANR-10-LABX-0039). E.C., H.A, C.D. and A.C. are supported by the ANR grant “BacFlow” ANR-15-CE30-0013. EC is supported by the Institut Universitaire de France. Declaration of Interests. The authors report no conflict of interest.

Appendix A. Track length statistics

The number of observed tracks decreases with time because tracks leave the observation window according to their average velocity. Figure 9 shows the number of tracks of non-motile and motile bacteria for the experiments at different flow rates as a function of time measured in units of the characteristic advection time τ_v , which here is the time to move over the characteristic grain length ℓ_0 by mean advection u_m . We see that the number of tracks decreases to around 90% of the initial number of tracks after around $2\tau_v$ for the non-motile and motile bacteria. After around $4\tau_v$ the number of tracks decreases to approximately 35% for the non-motile and to around 40% for the motile bacteria. This means, that the number of tracks of lengths larger than $4\ell_0$ is 35% and 40% of the total number of tracks. The long tracks are tortuous low velocity tracks that can be observed for a longer time. This is supported by the observation that the mean velocity starts decreasing after about $2\tau_v$, as shown in Figures 3 and 5 below. In the following, we consider travel times shorter than $5\tau_v$ in order to avoid too strong a bias toward slow bacteria. Even so, as we will see below, there is a significant slowing down of the mean displacement with increasing travel time, specifically for the motile bacteria.



h!

FIGURE 9. Number of tracks of (left panels) non-motile and (right panels) motile bacteria as a function of time.

Appendix B. Continuous time random walk model

The streamwise motion of a non-motile bacterium in the CTRW is described by Eq. (3.1). Unlike classical random walk strategies for the modeling of particle motion in heterogeneous flow fields, the CTRW approach models particle motion based on stochastic series of equidistant instead of isochronic particle speeds (e.g., Dentz *et al.* 2016; Morales *et al.* 2017), that is, particle speeds that change at equidistant points along a streamline. The streamwise displacement in the CTRW model represents the projection of the tortuous streamline onto the mean flow direction using advective tortuosity χ . This is illustrated schematically in Figure 10.

B.1. Non-motile bacteria

In the following, we provide a derivation of the Boltzmann-type equation (c) for the joint distribution $p(x, v, t)$ of particle displacement and speed. For more details, see Comoli *et al.* (2019). The distribution $p(x, v, t)$ can be written as

$$p(x, v, t) = \int_0^t dt' R(x, v, t') \int_{t-t'}^{\infty} dt'' \psi(t|v), \quad (\text{B1a})$$

where $\psi(t|v) = \delta(t - \Delta s/v)$. The probability per time $R(x, v, t)$ for the particle to just arrive at (x, v) at t satisfies

$$R(x, v, t) = R_0(x, v, t) + \int_0^t dt' \int dx' \int dv' \psi(x - x', t - t'|v') r(v|v') R(x', v', t'), \quad (\text{B1b})$$

where $r(v|v')$ is the transition probability from v' to v , and

$$\psi(x, t|v) = \delta(x - \Delta s/\chi) \delta(t - \Delta s/v). \quad (\text{B2})$$

The initial condition is encoded in $R_0(x, v, t)$, which is defined by

$$R_0(x, v, t) = p_0(x, v) \delta(t), \quad (\text{B3})$$

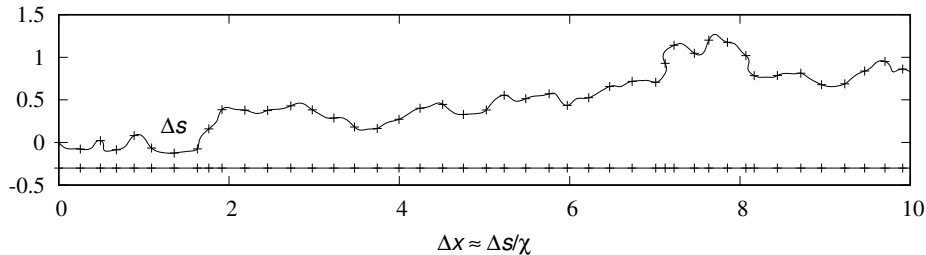


FIGURE 10. Schematic of the representation of a particle trajectory in the CTRW approach. Particles speeds are sampled equidistantly at turning points along a trajectory indicated by the constant Δs . The CTRW represents the trajectory projected onto the direction of the mean flow.

where $p_0(x, v)$ is the distribution of initial particle positions and speeds. Equations (B 1a) and (B 1b) can be combined in Laplace space to the generalized master equation

$$\lambda p^*(x, v, \lambda) = R_0^*(x, v, \lambda) + \int dx' \int dv' r(v|v') \left[\frac{\lambda \psi^*(x - x', \lambda|v')}{1 - \psi^*(\lambda|v')} p^*(x', v', \lambda) - \frac{\lambda \psi^*(\lambda|v)}{1 - \psi^*(\lambda|v)} p^*(x, v, \lambda) \right]. \quad (\text{B } 4)$$

Using the explicit form (B 2) for $\psi(x, t|v)$, it can be written as

$$\lambda p^*(x, v, \lambda) = R_0^*(x, v, \lambda) + \int dv' r(v|v') \frac{\lambda \exp(-\lambda \Delta s/v')}{1 - \exp(-\lambda \Delta s/v')} p^*(x - \Delta s/\chi, v', \lambda) - \frac{\lambda \exp(-\lambda \Delta s/v)}{1 - \exp(-\lambda \Delta s/v)} p^*(x, v, \lambda). \quad (\text{B } 5)$$

In the limit of $\Delta s \ll \ell_c$, we can write

$$\lambda p^*(x, v, \lambda) = R_0^*(x, v, \lambda) + \int dv' r(v|v') \left[\frac{v'}{\Delta s} p^*(x - \Delta s/\chi, v', \lambda) - \frac{v}{\Delta s} p^*(x, v, \lambda) \right] \quad (\text{B } 6)$$

$$= R_0^*(x, v, \lambda) + \int dv' r(v|v') \frac{v'}{\Delta s} p^*(x, v', \lambda) - \frac{v}{\chi} \frac{\partial}{\partial x} p^*(x, v, \lambda) - \frac{v}{\Delta s} p^*(x, v, \lambda), \quad (\text{B } 7)$$

where we localized $r(v|v') = \delta(v - v')$ in the advection term. By transformation back to time, we obtain the Boltzmann equation

$$\frac{\partial p(x, v, t)}{\partial t} + \frac{v}{\chi} \frac{\partial p(x, v, t)}{\partial x} = -\frac{v}{\Delta s} p(x, v, t) + \int_0^\infty dv' r(v|v') \frac{v'}{\Delta s} p(x, v', t'). \quad (\text{B } 8)$$

B.2. Motile bacteria

In the case of motile bacteria, we account for trapping during advective steps as well as initial trapping. Thus, we modify (B 1) as

$$p(x, v, t) = R_0(x, v, t) \int_t^\infty dt' \psi_0(t|v) + \int_0^t dt' R(x, v, t') \int_{t-t'}^\infty dt'' \psi_c(t|v). \quad (\text{B } 9a)$$

We define the initial transition probability

$$\psi_0(x, t|v) = (1 - \rho) \delta(x - \Delta s) \psi_c(t|v) + \rho \delta(x) \psi_f(t|v), \quad (\text{B } 9b)$$

and the distribution of initial transition times

$$\psi_0(t|v) = \int dx \psi_0(x, t|v) = (1 - \rho)\psi_c(t|v) + \rho\psi_f(t|v). \quad (\text{B } 9\text{c})$$

The distribution of compound transition times is given by

$$\psi_c(t|v) = \int_0^t dt' \psi(t'|v) \psi_c(t - t'|t'), \quad (\text{B } 9\text{d})$$

where $\psi_c(t - t'|t')$ is defined by (3.13). This relation reads in Laplace space as

$$\psi_c^*(\lambda|v) = \psi^*(\lambda[1 - \gamma\psi_f^*(\lambda)]) = \exp(-\lambda[1 - \gamma\psi_f^*(\lambda)]\Delta s/v). \quad (\text{B } 9\text{e})$$

The probability per time $R(x, v, t)$ for the particle to just arrive at (x, v) at t satisfies

$$R(x, v, t) = R_1(x, v, t) + \int_0^t dt' \int dx' \int dv' \psi_0(x - x', t - t'|v') r(v|v') R(x', v', t'), \quad (\text{B } 9\text{f})$$

where $r(v|v')$ is the transition probability from v' to v , and

$$\psi_c(x, t|v) = \delta(x - \Delta s)\psi_c(t|v). \quad (\text{B } 10)$$

The $R_1(x, v, t)$ is given by

$$R_1(x, v, t) = \int_0^t dt' \int dx' \int dv' \psi_0(x - x', t - t'|v') r(v|v') R_0(x', v', t'). \quad (\text{B } 11)$$

Equations (B 9a) and (B 9f) can be combined in Laplace space to the generalized master equation

$$\begin{aligned} \lambda G^*(x, v, \lambda) &= R_1^*(x, v, \lambda) + \int dv' r(v|v') \frac{\lambda \psi_c^*(\lambda|v')}{1 - \psi_c^*(\lambda|v')} G^*(x - \Delta s/\chi, v', \lambda) \\ &\quad - \frac{\lambda \psi_c^*(\lambda|v)}{1 - \psi_c^*(\lambda|v)} G^*(x, v, \lambda), \end{aligned} \quad (\text{B } 12)$$

where we defined

$$G^*(x, v, \lambda) = \left[p^*(x, v, \lambda) - R_0^*(x, v, \lambda) \frac{1 - \psi_0(\lambda|v)}{\lambda} \right]. \quad (\text{B } 13)$$

Using this definition and definition (B 11), we can write (B 12) as

$$\begin{aligned} \lambda p^*(x, v, \lambda) &= R_0^*(x, v, \lambda) \\ &+ \int dx' \int dv' r(v|v') [\psi_0^*(x - x', \lambda|v') R_0^*(x', v', \lambda) - \psi_0^*(\lambda|v) R_0^*(x, v, \lambda)] \\ &+ \int dv' r(v|v') \left[\frac{\lambda \psi_c^*(\lambda|v')}{1 - \psi_c^*(\lambda|v')} G^*(x - \Delta s/\chi, v', \lambda) - \frac{\lambda \psi_c^*(\lambda|v)}{1 - \psi_c^*(\lambda|v)} G^*(x, v, \lambda) \right]. \end{aligned} \quad (\text{B } 14)$$

Using the definition (B 9b) of $\psi_0(x, t|v)$, we obtain

$$\begin{aligned} \lambda p^*(x, v, \lambda) &= R_0^*(x, v, \lambda) \\ &+ \int dx' \int dv' r(v|v') (1 - \rho) [\psi_c^*(\lambda|v') R_0^*(x - \Delta s/\chi, v', \lambda) - \psi_c^*(\lambda|v) R_0^*(x, v, \lambda)] \\ &+ \int dv' r(v|v') \left[\frac{\lambda \psi_c^*(\lambda|v')}{1 - \psi_c^*(\lambda|v')} G^*(x - \Delta s/\chi, v', \lambda) - \frac{\lambda \psi_c^*(\lambda|v)}{1 - \psi_c^*(\lambda|v)} G^*(x, v, \lambda) \right]. \end{aligned} \quad (\text{B } 15)$$

Note that

$$\begin{aligned} & \frac{\lambda\psi_c^*(\lambda|v)}{1-\psi_c^*(\lambda|v)}R_0^*(x,v,\lambda)\frac{1-\psi_0(\lambda|v)}{\lambda} \\ &= R_0^*(x,v,\lambda)(1-\rho)\psi_c^*(\lambda|v) + \rho R_0^*(x,v,\lambda)\frac{\psi_c^*(\lambda|v)}{1-\psi_c^*(\lambda|v)}\phi^*(\lambda), \end{aligned} \quad (\text{B } 16)$$

where we defined

$$\phi^*(\lambda) = \frac{1-\psi_f^*(\lambda)}{\lambda}. \quad (\text{B } 17)$$

Combining everything, we obtain

$$\begin{aligned} \lambda p^*(x,v,\lambda) &= R_0^*(x,v,\lambda) + \int dv' r(v|v') \frac{\lambda\psi_c^*(\lambda|v')}{1-\psi_c^*(\lambda|v')} G_m^*(x-\Delta s/\chi, v', \lambda) \\ &\quad - \frac{\lambda\psi_c^*(\lambda|v)}{1-\psi_c^*(\lambda|v)} G_m^*(x,v,\lambda), \end{aligned} \quad (\text{B } 18)$$

where we defined

$$G_m^*(x,v,\lambda) = p^*(x,v,\lambda) - \rho R_0^*(x,v,\lambda)\phi^*(\lambda). \quad (\text{B } 19)$$

Furthermore, we approximate for small Δs

$$\frac{\psi_c^*(\lambda|v)}{1-\psi_c^*(\lambda|v)} = \frac{v}{\Delta s} \frac{1}{1+\gamma\phi^*(\lambda)} \quad (\text{B } 20)$$

Thus, we obtain

$$\begin{aligned} \lambda p^*(x,v,\lambda) &= R_0^*(x,v,\lambda) + \int dv' r(v|v') \frac{v'}{\Delta s} \frac{G_m^*(x-\Delta s/\chi, v', \lambda)}{1+\gamma\phi^*(\lambda)} \\ &\quad - \frac{v}{\Delta s} \frac{G_m^*(x,v,\lambda)}{1+\gamma\phi^*(\lambda)}, \end{aligned} \quad (\text{B } 21)$$

We define now the mobile concentration of bacteria in the stream as

$$p_s^*(x,v,\lambda) = \frac{G_m^*(x,v,\lambda)}{1+\gamma\phi^*(\lambda)} = \frac{p^*(x,v,\lambda) - \rho R_0^*(x,v,\lambda)\phi^*(\lambda)}{1+\gamma\phi^*(\lambda)} \quad (\text{B } 22)$$

With this definition, we obtain

$$\begin{aligned} \lambda[1+\gamma\phi^*(\lambda)]p_s^*(x,v,\lambda) &= R_0^*(x,v,\lambda) - \rho\lambda R_0^*(x,v,\lambda)\phi^*(\lambda) \\ &\quad + \int dv' r(v|v') \left[\frac{v'}{\Delta s} p_s^*(x-\Delta s/\chi, v', \lambda) - \frac{v}{\Delta s} p_s^*(x,v,\lambda) \right], \end{aligned} \quad (\text{B } 23)$$

Expanding the integral terms on the right side in analogy to the previous section gives

$$\begin{aligned} \lambda[1+\gamma\phi^*(\lambda)]p_s^*(x,v,\lambda) &= R_0^*(x,v,\lambda) - \rho\lambda R_0^*(x,v,\lambda)\phi^*(\lambda) \\ &\quad + \int dv' r(v|v') \frac{v'}{\Delta s} p_s^*(x, v', \lambda) - \frac{v}{\chi} \frac{\partial}{\partial x} p_s^*(x,v,\lambda) - \frac{v}{\Delta s} p_s^*(x,v,\lambda), \end{aligned} \quad (\text{B } 24)$$

By transformation back to time, we obtain the Boltzmann equation

$$\begin{aligned} \frac{\partial p_s(x, v, t)}{\partial t} + \frac{\partial}{\partial t} \int_0^t dt' \gamma \phi(t-t') p_s(x, t') + \frac{v}{\chi} \frac{\partial p(x, v, t)}{\partial x} = \\ \rho p_0(x, v) \psi_f(t) - \frac{v}{\Delta s} p(x, v, t) + \int_0^\infty dv' r(v|v') \frac{v'}{\Delta s} p(x, v', t'). \end{aligned} \quad (\text{B } 25)$$

Appendix C. Initial trapping time distribution

In order to derive the initial trapping time distribution, we employ the concept of the backward recurrence time $B_{t_0} = t_0 - t_N$, this means the time that has passed between a target time t_0 and the time t_N of the last trapping event before t_0 . For a Poissonian trapping process, this means for an exponential inter-event time distribution, the distribution of B_{t_0} in the steady state limit, that is, for $N \rightarrow \infty$, is given by (Godrèche & Luck 2001)

$$\psi_B(t) = \gamma \exp(-\gamma t). \quad (\text{C } 1)$$

It is independent from t_0 , $B_{t_0} \equiv B$. The initial trapping time η_0 can be expressed in terms of B as $\eta_0 = \tau_f - B$. Thus, the joint distribution for a bacterium to be trapped and have the trapping time $\eta_0 < t$ is

$$\text{Prob}(\eta_0 < t \wedge \text{trapped}) = \langle H(\tau_f - B) H[t - (\tau_f - B)] \rangle \quad (\text{C } 2)$$

It can be written as

$$\text{Prob}(\eta_0 < t \wedge \text{trapped}) = \int_0^\infty dt' \int_0^\infty dt'' H(t' - t'') H[t - (t' - t'')] \psi_B(t'') \psi_f(t'). \quad (\text{C } 3)$$

Using expression (C 1) for $\psi_B(t)$ and shifting $t'' \rightarrow t' - t''$, we obtain

$$\begin{aligned} \text{Prob}(\eta_0 < t \wedge \text{trapped}) &= \int_0^\infty dt' \int_0^\infty dt'' \gamma \exp[-\gamma(t' - t'')] \psi_f(t') H(t - t'') H(t' - t'') \\ &= \int_0^t dt'' \int_{t''}^\infty dt' \gamma \exp[-\gamma(t' - t'')] \psi_f(t') \end{aligned} \quad (\text{C } 4)$$

Thus we obtain for the joint probability of being trapped and η_0 in $[t, t+dt]$ by derivation of (C 4) with respect to t

$$P_0(t) = \int_t^\infty dt' \gamma \exp[-\gamma(t' - t)] \psi_f(t') \quad (\text{C } 5)$$

For $\psi_f(t) = \exp(-t/\tau_c)/\tau_c$, we obtain

$$\begin{aligned} \text{Prob}(\eta_0 < t \wedge \text{trapped}) &= \int_0^t dt'' \int_{t''}^\infty dt' \gamma \tau_c^{-1} \exp[\gamma t'' - t'(\tau_c^{-1} + \gamma)] \\ &= \frac{\gamma \tau_c}{1 + \gamma \tau_c} \exp(-t/\tau_c). \end{aligned} \quad (\text{C } 6)$$

Appendix D. Asymptotic dispersion and retardation coefficients for motile bacteria

In order to derive the dispersion and retardation coefficients for motile bacteria, we consider the Fourier-Laplace transform of the total bacteria distribution $p(x, t) = p_s(x, t) + p_g(x, t)$. From the Fourier-Laplace transform of (3.23), we obtain

$$\tilde{p}^*(k, \lambda) = \tilde{p}_s^*(k, \lambda) [1 + \phi^*(\lambda)\gamma] + \rho\phi^*(\lambda). \quad (\text{D } 1)$$

The Fourier-Laplace transform of the density $p_s(x, t)$ in the stream is obtained from (3.22) as

$$\tilde{p}_s^*(k, \lambda) = \frac{1 - \rho\lambda\phi^*(\lambda)}{\lambda [1 + \phi^*(\lambda)\gamma] - iku_m + D_{nm}k^2}, \quad (\text{D } 2)$$

where we used Eq. (B 17) to express $\psi_f^*(\lambda)$ in terms of $\phi^*(\lambda)$. The Laplace transforms of the mean and mean square displacements are given in terms of $\tilde{p}^*(k, \lambda)$ as

$$m_n^*(\lambda) = (-i)^n \left. \frac{\partial^n \tilde{p}^*(k, \lambda)}{\partial k^n} \right|_{k=0} \quad (\text{D } 3)$$

for $n = 1, 2$. Using (D 1), we obtain

$$m_n^*(\lambda) = (-i)^n \left. \frac{\partial^n \tilde{p}_s^*(k, \lambda)}{\partial k^n} \right|_{k=0} [1 + \phi^*(\lambda)\gamma]. \quad (\text{D } 4)$$

Using (D 2), we obtain the explicit expressions

$$m_1^*(\lambda) = \frac{u_m}{\lambda^2} \frac{1 - \rho\lambda\phi^*(\lambda)}{[1 + \phi^*(\lambda)\gamma]} \quad (\text{D } 5)$$

$$m_2^*(\lambda) = \frac{2D}{\lambda^2} \frac{1 - \rho\lambda\phi^*(\lambda)}{[1 + \phi^*(\lambda)\gamma]} + \frac{2u_m^2}{\lambda^3} \frac{1 - \rho\lambda\phi^*(\lambda)}{[1 + \phi^*(\lambda)\gamma]^2} \quad (\text{D } 6)$$

We set now $\rho = \beta/(1 + \beta)$ with $\beta = \gamma\tau_c$ and $\phi(t) = \exp(-t/\tau_c)$, which implies

$$\phi^*(\lambda) = \frac{\tau_c}{1 + \lambda\tau_c}. \quad (\text{D } 7)$$

Thus, we obtain

$$m_1^*(\lambda) = \frac{u_m}{(1 + \beta)\lambda^2} \quad (\text{D } 8)$$

$$m_2^*(\lambda) = \frac{2D_{nm}}{(1 + \beta)\lambda^2} + \frac{2u_m^2}{(1 + \beta)^2\lambda^3} \frac{1 + \lambda\tau_c}{1 + \lambda\frac{\tau_c}{1 + \beta}} \quad (\text{D } 9)$$

The latter can be written as

$$m_2^*(\lambda) = \frac{2D_{nm}}{(1 + \beta)\lambda^2} + \frac{2u_m^2}{(1 + \beta)^2\lambda^3} + \frac{2u_m^2\beta\tau_c}{(1 + \beta)^3\lambda^2} \frac{1}{1 + \lambda\frac{\tau_c}{1 + \beta}} \quad (\text{D } 10)$$

In the limit of $\lambda\tau_c \rightarrow 0$, we obtain in leading order

$$m_2^*(\lambda) = \frac{2D_{nm}}{(1 + \beta)\lambda^2} + \frac{2u_m^2}{(1 + \beta)^2\lambda^3} + \frac{2u_m^2\beta\tau_c}{(1 + \beta)^3\lambda^2} \quad (\text{D } 11)$$

Inverse Laplace transform gives

$$m_1(t) = \frac{u_m t}{1 + \beta} \quad (\text{D 12})$$

$$m_2(t) = \frac{2D_{nm}t}{1 + \beta} + \frac{u_m^2 t^2}{(1 + \beta)^2} + \frac{2u_m^2 \beta \tau_c}{(1 + \beta)^3} \quad (\text{D 13})$$

We define the retardation coefficient by comparing $m_1(t)$ with the mean displacement for the non-motile bacteria. This gives

$$R = 1 + \beta. \quad (\text{D 14})$$

The displacement variance is given by

$$\sigma^2(t) = \frac{2D_{nm}t}{R} + \frac{2u_m^2 \tau_c (R - 1)t}{R^3} \quad (\text{D 15})$$

Thus, we obtain for the dispersion coefficient

$$D_m = \frac{D_{nm}}{R} + \frac{u_m^2 \tau_c (R - 1)}{R^3} \quad (\text{D 16})$$

We consider now the asymptotic equation for the total bacteria concentration. Thus, we consider the Fourier-Laplace transform of the total bacteria distribution $p(x, t) = p_s(x, t) + p_g(x, t)$. From the Fourier-Laplace transform of (3.23), we obtain

$$\tilde{p}_s^*(k, \lambda) = \frac{\tilde{p}^*(k, \lambda) - \rho \phi^*(\lambda)}{[1 + \phi^*(\lambda)\gamma]}. \quad (\text{D 17})$$

Thus, we obtain from (3.22)

$$\lambda \tilde{p}^*(k, \lambda) - \left(iku_m - D_{nm}k^2\right) \frac{\tilde{p}^*(k, \lambda) - \rho \phi^*(\lambda)}{1 + \phi^*(\lambda)\gamma} = 1, \quad (\text{D 18})$$

where we used Eq. (B17) to express $\psi_f^*(\lambda)$ in terms of $\phi^*(\lambda)$. We use the expansion

$$\phi^*(\lambda) = \tau_c (1 - \lambda \tau_c). \quad (\text{D 19})$$

in order to expand (D 18) up to linear order in λ

$$\lambda \tilde{p}^*(k, \lambda) - \frac{iku_m - D_{nm}k^2}{1 + \gamma \tau_c} \tilde{p}^*(k, \lambda) \left(1 - \frac{\lambda \gamma \tau_c^2}{1 + \gamma \tau_c}\right) = 1, \quad (\text{D 20})$$

where we disregard terms of order $k\phi^*(\lambda)$ and order λ^2 . We set now self-consistently

$$\lambda \tilde{p}^*(k, \lambda) = 1 + \frac{iku_m}{1 + \gamma \tau_c} \tilde{p}^*(k, \lambda) \quad (\text{D 21})$$

to obtain

$$\lambda \tilde{p}^*(k, \lambda) - \frac{iku_m - D_{nm}k^2}{1 + \gamma \tau_c} \tilde{p}^*(k, \lambda) + \frac{u_m^2 \gamma \tau_c^2 k^2}{(1 + \gamma \tau_c)^3} \tilde{p}^*(k, \lambda) = 1, \quad (\text{D 22})$$

where we disregard terms of order k . Using definitions (D 14) and (D 16), we obtain

$$\lambda \tilde{p}^*(k, \lambda) - \left(ik \frac{u_m}{R} - D_m k^2\right) \tilde{p}^*(k, \lambda) = 1. \quad (\text{D 23})$$

The inverse Fourier-Laplace transform of this equation gives Eq. (3.24).

Appendix E. Physical model for bacteria blow-off from grains

A simple model is proposed with the objective of showing that the characteristic residence time τ_c is inversely proportional to the average flow velocity. Let's consider a circular obstacle of size l_0 facing a flow of average velocity U . The flow field around the grain is given by

$$v_r = U \left(1 - \frac{\ell_0^2}{4r^2} \right) \cos(\theta) \quad (\text{E1})$$

$$v_\theta = -U \left(1 + \frac{\ell_0^2}{4r^2} \right) \sin(\theta), \quad (\text{E2})$$

where r is the distance from the center of the grain and θ the angle with respect to the flow direction. The shear rate on the grain surface is:

$$\dot{\gamma} = \left. \frac{\partial v_\theta}{\partial r} \right|_{r=\frac{\ell_0}{2}} = \frac{4U}{\ell_0} \sin(\theta) \quad (\text{E3})$$

Bacteria transported in the vicinity of the grain rotate because of the local shear. Because of their swimming ability, some are able to reach the rear of the obstacles where the flow is low (Miño et al. 2018). Once on the surface, the bacteria body aligns with the surface and hydrodynamic interaction favors their swimming along the surface. Hydrodynamic interactions are known to influence the bacteria over a distance δ of the order of ten microns (Berke et al. 2008; Li et al. 2011). As they move upstream along the surface, they face an increasing shear rate. When the shear rate reaches the critical value of $\dot{\gamma}_c \sim 5s^{-1}$, the bacteria are stopped by the flow and are eventually detached from the surface and returned to the flow. This scenario is based on the video available in the supplemental material section of Creppy et al. (2019). This video shows motile bacteria (white rods) transported by a flow (average velocity $72 \mu m/s$). On the video, the upstream displacements are clearly identifiable as well as the motion towards the rear of the grains and the displacements on the surfaces and the final release. This succession of steps was also recently identified by computer simulations using molecular dynamics coupled with lattice Boltzmann (Lee et al. 2021) as the scenario characterizing the entrapment and release of motile bacteria moving near an obstacle.

The critical shear rate is reached when $\theta = \arcsin(\dot{\gamma}_c \ell_0 / 4U)$. The model requires a minimal mean flow velocity $U_c = \frac{\ell_0 \dot{\gamma}_c}{4}$, below which diffusion of the bacteria due to the swimming activity dominates. The minimal fluid velocity required to see the separation between bacteria moving on the grains and in the pore channels is about $30 \mu m/s$. Above this velocity, the total distance swum by the bacteria on the grain surface before its release is $l \sim \ell_0 \theta / 2$ if θ is not too large. The motion on the grain is at swimming velocity v_0 and the total time to swim from the back of the grain to the critical angle is $\tau_c = \frac{\ell_0^2 \dot{\gamma}_c}{8v_0} \frac{1}{U}$. We recover here the scaling obtained from interpretation of the data by the CTRW model.

REFERENCES

- ALIM, KAREN, PARSA, SHIMA, WEITZ, DAVID A. & BRENNER, MICHAEL P. 2017 Local pore size correlations determine flow distributions in porous media. *Physical Review Letters* **119** (14).
- ALONSO-MATILLA, ROBERTO, CHAKRABARTI, BRATO & SAINTILLAN, DAVID 2019 Transport and dispersion of active particles in periodic porous media. *Phys. Rev. Fluids* **4**, 043101.
- ALTSHULER, E., MIÑO, G., PÉREZ-PENICHER, C., RÍO, L. DEL, LINDNER, A., ROUSSELET, A.

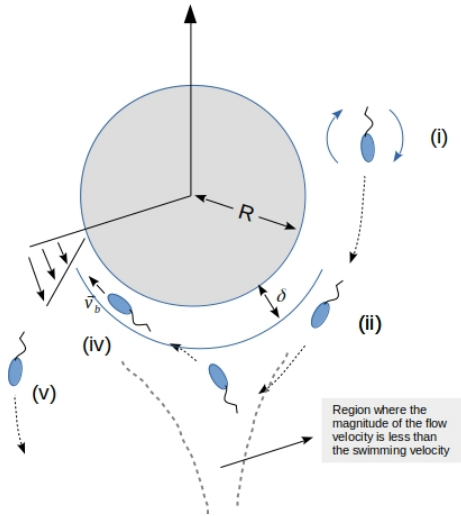


FIGURE 11. Illustration of the model. (i) because of the local shear, the bacteria rotates in the flow (ii) some are redirected towards the rear of the grain where the flow velocity is small (iii) the bacteria swims towards the grain and then along the surface. As they move along the grain they face an increase local shear rate. When the shear become larger than a critical value $\dot{\gamma}_c$, the bacteria gets blow and goes back to the flow.

- & CLÉMENT, E. 2013 Flow-controlled densification and anomalous dispersion of *e. coli* through a constriction. *Soft Matter* **9** (6), 1864–1870.
- DE ANNA, PIETRO, PAHLAVAN, AMIR A., YAWATA, YUTAKA, STOCKER, ROMAN & JUANES, RUBEN 2020 Chemotaxis under flow disorder shapes microbial dispersion in porous media. *Nature Physics* **17** (1), 68–73.
- ARAMIDEH, SOROUSH, VLACHOS, PAVLOS P. & ARDEKANI, AREZOO M. 2018 Pore-scale statistics of flow and transport through porous media. *Physical Review E* **98** (1).
- BAI, HONGJUAN, COCHET, NELLY, PAUSS, ANDRÉ & LAMY, EDVINA 2016 Bacteria cell properties and grain size impact on bacteria transport and deposition in porous media. *Colloids and Surfaces B: Biointerfaces* **139**, 148–155.
- BEAR, J. 1972 Dynamics of fluids in porous media. American Elsevier, New York.
- BECKER, MATTHEW W., METGE, DAVID W., COLLINS, SAMANTHA A., SHAPIRO, ALLEN M. & HARVEY, RONALD W. 2003 Bacterial transport experiments in fractured crystalline bedrock. *Ground Water* **41** (5), 682–689.
- BERG, HOWARD C 2018 Random walks in biology. In Random Walks in Biology. Princeton University Press.
- BERKE, ALLISON P., TURNER, LINDA, BERG, HOWARD C. & LAUGA, ERIC 2008 Hydrodynamic attraction of swimming microorganisms by surfaces **101** (3).
- BERKOWITZ, B. & SCHER, H. 1997 Anomalous transport in random fracture networks. *Phys. Rev. Lett.* **79** (20), 4038–4041.
- BRENNER, H. & EDWARDS, D. 1993 Macrotransport Processes. Butterworth-Heinemann, MA, USA.
- CAMESANO, TERRI A. & LOGAN, BRUCE E. 1998 Influence of fluid velocity and cell concentration on the transport of motile and nonmotile bacteria in porous media. *Environmental Science & Technology* **32** (11), 1699–1708.
- CARREL, MAXENCE, MORALES, VERÓNICA L, DENTZ, MARCO, DERLON, NICOLAS, MORGENROTH, EBERHARD & HOLZNER, MARKUS 2018 Pore-scale hydrodynamics in a progressively bioclogged three-dimensional porous medium: 3-d particle tracking experiments and stochastic transport modeling. *Water resources research* **54** (3), 2183–2198.
- COMOLLI, ALESSANDRO, HAKOUN, VIVIEN & DENTZ, MARCO 2019 Mechanisms, upscaling,

- and prediction of anomalous dispersion in heterogeneous porous media. *Water Resources Research* **55** (10), 8197–8222.
- CREPPY, ADAMA, CLÉMENT, ERIC, DOUARCHE, CARINE, D'ANGELO, MARIA VERONICA & AURADOU, HAROLD 2019 Effect of motility on the transport of bacteria populations through a porous medium. *Phys. Rev. Fluids* **4**, 013102.
- DARCY, HENRY 1856 Les fontaines publiques de la ville de Dijon: exposition et application.... Victor Dalmont.
- DE ANNA, P., QUAIFE, B., BIROS, G. & JUANES, R. 2017 Prediction of velocity distribution from pore structure in simple porous media. *Phys. Rev. Fluids* **2**, 124103.
- DEHKHARGHANI, AMIN, WAISBORD, NICOLAS, DUNKEL, JÖRN & GUASTO, JEFFREY S. 2019 Bacterial scattering in microfluidic crystal flows reveals giant active taylor–aris dispersion. *Proceedings of the National Academy of Sciences* **116** (23), 11119–11124.
- DENTZ, MARCO & BERKOWITZ, BRIAN 2003 Transport behavior of a passive solute in continuous time random walks and multirate mass transfer. *Water Resources Research* **39** (5).
- DENTZ, M., ICARDI, M. & HIDALGO, J. J. 2018 Mechanisms of dispersion in a porous medium. *J. Fluid Mech.* **841**, 851–882.
- DENTZ, MARCO, KANG, PETER K, COMOLLI, ALESSANDRO, LE BORGNE, TANGUY & LESTER, DANIEL R 2016 Continuous time random walks for the evolution of lagrangian velocities. *Physical Review Fluids* **1** (7), 074004.
- FELLER, W. 1968 An Introduction to Probability Theory and Its Applications, *Wiley Series in Probability and Statistics*, vol. 1. Wiley.
- FIGUEROA-MORALES, NURIS, LEONARDO MIÑO, GASTÓN, RIVERA, ARAMIS, CABALLERO, ROGELIO, CLÉMENT, ERIC, ALTSHULER, ERNESTO & LINDNER, ANKE 2015 Living on the edge: transfer and traffic of e. coli in a confined flow. *Soft Matter* **11** (31), 6284–6293.
- FIGUEROA-MORALES, NURIS, RIVERA, ARAMIS, SOTO, RODRIGO, LINDNER, ANKE, ALTSHULER, ERNESTO & CLÉMENT, ÉRIC 2020a E. coli “super-contaminates” narrow ducts fostered by broad run-time distribution. *Science Advances* **6** (11).
- FIGUEROA-MORALES, NURIS, SOTO, RODRIGO, JUNOT, GASPARD, DARNIGE, THIERRY, DOUARCHE, CARINE, MARTINEZ, VINCENT A, LINDNER, ANKE & CLÉMENT, ERIC 2020b 3d spatial exploration by e. coli echoes motor temporal variability. *Physical Review X* **10** (2), 021004.
- GHANBARIAN, BEHZAD, HUNT, ALLEN G., EWING, ROBERT P. & SAHIMI, MUHAMMAD 2013 Tortuosity in porous media: A critical review. *Soil Science Society of America Journal* **77** (5), 1461–1477.
- GODRÈCHE, C. & LUCK, J. M. 2001 Statistics of the occupation time of renewal processes. *Journal of Statistical Physics* **104** (3/4), 489–524.
- HENDRY, M. J., LAWRENCE, J. R. & MALOSZEWSKI, P. 1999 Effects of velocity on the transport of two bacteria through saturated sand. *Ground Water* **37** (1), 103–112.
- HOLZNER, MARKUS, MORALES, VERÓNICA L, WILLMANN, MATTHIAS & DENTZ, MARCO 2015 Intermittent Lagrangian velocities and accelerations in three-dimensional porous medium flow. *Physical Review E* **92** (1), 013015.
- HORNBERGER, G.M., MILLS, A.L. & HERMAN, J.S. 1992 Bacterial transport in porous media evaluation of a model using laboratory observation. *Water Resources Research* pp. 915–938.
- HYMAN, JEFFREY D., RAJARAM, HARIHAR, SRINIVASAN, SHRIRAM, MAKEDONSKA, NATALIJA, KARRA, SATISH, VISWANATHAN, HARI & SRINIVASAN, GOWRI 2019 Matrix diffusion in fractured media: New insights into power law scaling of breakthrough curves. *Geophysical Research Letters* **46** (23), 13785–13795.
- JEFFERY, G.B. 1922 The motion of ellipsoidal particles immersed in a viscous fluid. *Proceedings of the Royal Society of London. Series A, Containing Papers of a Mathematical and Physical Character* **102** (715), 161–179.
- JIANG, GUANGMING, NOONAN, MIKE J., BUCHAN, GRAEME D. & SMITH, NEIL 2005 Transport and deposition of bacillus subtilis through an intact soil column. *Australian Journal of Soil Research* , **43**, 695–703.
- JING, GUANGYIN, ZÖTTL, ANDREAS, CLÉMENT, ÉRIC & LINDNER, ANKE 2020 Chirality-induced bacterial rheotaxis in bulk shear flows. *Science Advances* **6** (28), eabb2012.

- DE JOSSELINE DE JONG, G. 1958 Longitudinal and transverse diffusion in granular deposits. *Trans. Amer. Geophys. Un.* **39**, 67–74.
- JUNOT, GASPARD, DARNIGE, THIERRY, LINDNER, ANKE, MARTINEZ, VINCENT A., ARLT, JOCHEN, DAWSON, ANGELA, POON, WILSON C. K., AURADOU, HAROLD & CLÉMENT, ERIC 2021 Run-to-tumble variability controls the surface residence times of *e. coli* bacteria.
- KAYA, TOLGA & KOSER, HUR 2012 Direct upstream motility in escherichia coli. *Biophysical Journal* **102** (7), 1514–1523.
- KOPONEN, A., KATAJA, M. & TIMONEN, J. 1996 Tortuous flow in porous media. *Phys. Rev. E* **54**, 406–410.
- LEE, MIRU, LOHRMANN, CHRISTOPH, SZUTTOR, KAI, AURADOU, HAROLD & HOLM, CHRISTIAN 2021 The influence of motility on bacterial accumulation in a microporous channel. *Soft Matter* **17** (4), 893–902.
- LI, GUANGLAI, BENSSON, JAMES, NISIMOVA, LIANA, MUNGER, DANIEL, MAHAUTMR, PANRAPEE, TANG, JAY X., MAXEY, MARTIN R. & BRUN, YVES V. 2011 Accumulation of swimming bacteria near a solid surface. *Physical Review E* **84** (4), 041932.
- LIANG, XIAOMENG, LU, NANXI, CHANG, LIN-CHING, NGUYEN, THANH H. & MASSOUDIEH, ARASH 2018 Evaluation of bacterial run and tumble motility parameters through trajectory analysis **211**, 26–38.
- LIU, JUN, FORD, ROSEANNE M. & SMITH, JAMES A. 2011 Idling time of motile bacteria contributes to retardation and dispersion in sand porous medium **45** (9), 3945–3951.
- MARCOS, FU, HENRY C., POWERS, THOMAS R. & STOCKER, ROMAN 2012 Bacterial rheotaxis. *Proceedings of the National Academy of Sciences* **109** (13), 4780–4785.
- MARGOLIN, GENNADY, DENTZ, MARCO & BERKOWITZ, BRIAN 2003 Continuous time random walk and multirate mass transfer modeling of sorption. *Chemical Physics* **295** (1), 71–80.
- MATHIJSEN, ARNOLD J. T. M., FIGUEROA-MORALES, NURIS, JUNOT, GASPARD, CLÉMENT, ÉRIC, LINDNER, ANKE & ZÖTTL, ANDREAS 2019 Oscillatory surface rheotaxis of swimming *e. coli* bacteria. *Nature Communications* **10** (1), 1–12.
- MATYKA, M., GOLEMBIEWSKI, J. & KOZA, Z. 2016 Power-exponential velocity distributions in disordered porous media. *Phys. Rev. E* **93**, 013110.
- MCCAULOU, DOUGLAS R., BALES, ROGER C. & MCCARTHY, JOHN F. 1994 Use of short-pulse experiments to study bacteria transport through porous media. *Journal of contaminant hydrology* **15** (1), 1–14.
- MIÑO, GASTÓN L., BAABOUR, MAGALI, CHERTCOFF, RICARDO, GUTKIND, GABRIEL, CLÉMENT, ERIC, AURADOU, HAROLD & IPPOLITO, IRENE 2018 *E coli* accumulation behind an obstacle. *Advances in Microbiology* **08** (6), 451.
- MORALES, VERONICA L, DENTZ, MARCO, WILLMANN, MATTHIAS & HOLZNER, MARKUS 2017 Stochastic dynamics of intermittent pore-scale particle motion in three-dimensional porous media: Experiments and theory. *Geophysical Research Letters* **44** (18), 9361–9371.
- NOETINGER, BENOIT, ROUBINET, DELPHINE, RUSSIAN, ANNA, LE BORGNE, TANGUY, DELAY, FREDERICK, DENTZ, MARCO, DE DREUZY, JEAN-RAYNALD & GOUZE, PHILIPPE 2016 Random walk methods for modeling hydrodynamic transport in porous and fractured media from pore to reservoir scale. *Transport in Porous Media* **115** (2), 345–385.
- PUYGUIRAUD, ALEXANDRE, GOUZE, PHILIPPE & DENTZ, MARCO 2019a Stochastic dynamics of lagrangian pore-scale velocities in three-dimensional porous media. *Water Resources Research* **55** (2), 1196–1217.
- PUYGUIRAUD, ALEXANDRE, GOUZE, PHILIPPE & DENTZ, MARCO 2019b Upscaling of anomalous pore-scale dispersion. *Transport in Porous Media* **128** (2), 837–855.
- PUYGUIRAUD, ALEXANDRE, GOUZE, PHILIPPE & DENTZ, MARCO 2021 Pore-scale mixing and the evolution of hydrodynamic dispersion in porous media. *Physical Review Letters* **126** (16), 164501.
- RUSCONI, ROBERTO, GUASTO, JEFFREY S. & STOCKER, ROMAN 2014 Bacterial transport suppressed by fluid shear. *Nature Physics* **10** (3), 212–217.
- SAFFMAN, PG 1959 A theory of dispersion in a porous medium. *Journal of Fluid Mechanics* **6** (03), 321–349.
- SCHIEDWEILER, DAVID, MIELE, FILIPPO, PETER, HANNES, BATTIN, TOM J. & DE ANNA, PIETRO 2020 Trait-specific dispersal of bacteria in heterogeneous porous environments:

- from pore to porous medium scale. *Journal of The Royal Society Interface* **17** (164), 20200046.
- SECCHI, ELEONORA, VITALE, ALESSANDRA, MIÑO, GASTÓN L., KANTSLEER, VASILY, EBERL, LEO, RUSCONI, ROBERTO & STOCKER, ROMAN 2020 The effect of flow on swimming bacteria controls the initial colonization of curved surfaces. *Nature Communications* **11** (1).
- SIENA, M, RIVA, M, HYMAN, JD, WINTER, C LARRABEE & GUADAGNINI, A 2014 Relationship between pore size and velocity probability distributions in stochastically generated porous media. *Physical Review E* **89** (1), 013018.
- SOUZY, M., LHUISSIER, H., MÉHEUST, Y., BORGNE, T. LE & METZGER, B. 2020 Velocity distributions, dispersion and stretching in three-dimensional porous media. *Journal of Fluid Mechanics* **891**.
- STUMPP, CHRISTINE, LAWRENCE, JOHN R., HENDRY, M. JIM & MALOSZEWSKI, PIOTR 2011 Transport and bacterial interactions of three bacterial strains in saturated column experiments. *Environmental Science & Technology* **45** (6), 2116–2123.
- TAYLOR, G. I. 1953 Dispersion of soluble matter in solvent flowing slowly through a tube. *Proc. R. Soc. Lond. A* **219**, 186–203.
- TUFENKJI, NATHALIE 2007 Modeling microbial transport in porous media: Traditional approaches and recent developments. *Advances in Water Resources* **30** (6), 1455–1469.
- WALKER, SHARON L., REDMAN, JEREMY A. & ELIMELECH, MENACHEM 2005 Influence of growth phase on bacterial deposition: Interaction mechanisms in packed-bed column and radial stagnation point flow systems. *Environmental Science & Technology* **39** (17), 6405–6411.
- YATES, MARYLYNN V., YATES, SCOTT R. & GERBA, CHARLES P. 1988 Modeling microbial fate in the subsurface environment. *Critical Reviews in Environmental Control* **17** (4), 307–344.
- ZHANG, MENGYA, HE, LEI, JIN, XIN, BAI, FAN, TONG, MEIPING & NI, JINREN 2021 Flagella and their properties affect the transport and deposition behaviors of escherichia coli in quartz sand. *Environmental Science & Technology* **55** (8), 4964–4973.